Relating ECoG and the local field potential to underlying mechanisms

Meron Vermaas[a]

[a]*Master Neuroscience & Cognition, Graduate School of Life Sciences, Utrecht University, Utrecht, The Netherlands*

Abstract

Since the advent of multielectrodes, interest in the low-frequency part of the extracellular field potential (EFP) has surged. Interpreting this electric signal is complicated because it is a superposition of transmembrane currents originating from multiple neuronal processes. The magnitude and shape of the recorded potential are dependent on factors such as the dynamics of the individual sources generating the currents, the amount of synchrony in synaptic activity and the neuron morphology. Here the relation between the EFP and its underlying mechanisms is addressed based on literature studying the signal intracranially (electrocorticogram, ECoG) and intracortically (local field potentials, LFPs). The traditional approach of decomposing the EFP signal based on the power spectrum of the frequencies is evaluated. Several alternatives more sensitive to dissociate between different frequency bands are suggested such as the matching pursuit algorithm and optimization techniques. Furthermore, mathematical modeling schemes are used to describe quantitatively how factors like synchrony and cytoarchitecture affect characteristics of the EFP and how different current sources contribute to the signal. These modeling studies are suggested as a means to predict limitations and optimum experimental stimuli for measurements such as ECoG. Simulating and combining experimental data recorded at different spatial scales with reconstructed neuronal tissue is necessary to optimally make use of the network signaling information embedded in the EFP and is essential for future progress.

Layman's summary.
When the brain is active, currents are generated which can be recorded as an electric signal with a carefully positioned electrode. The signal that is measured when the electrode is placed outside of the cell is called the extracellular field potential (EFP). It can be measured at different locations, for example on the scalp, under the skull or inside the brain. This electric signal picks up many different processes that happen in the brain, which makes it difficult to interpret. To understand the EFP, one must know what kind of neural mechanisms contribute to the signal. In addition, the structure of the brain and the shape of neurons have to be taken into account because they affect how the individual contributions are measured. In this study, we describe and evaluate mathematical modeling schemes and analyses of the EFP which are key to a better understanding of its origins. For example, careful analysis of recorded EFPs demonstrates how some parts of the signal seem to reflect the output activity of neurons. Using a modeling formula, it can be shown that the magnitude of the signal depends on the amount of synchrony of the activity in the neurons. Ultimately, combining models of the EFP with real data may provide more insight into neuronal processing and show how to design future experiments to optimally study cognition and perception.

1. Introduction

Neuronal networks and their dynamics are assumed to underlie behavior and cognition. In order better to understand neuronal activity and the behavior it generates, measurements at different temporal and spatial scales must be combined. Cortical electrical currents have long been at the center of attention, since at least 1875 (Caton, 1875), which is several decades before the first electroencephalography (EEG) recording (Pravdich-Neminsky, 1913). EEG measures at a macroscopic scale and is the principal method used to sample activity from many cortical populations. Microscopic electrophysiological experiments have focused primarily on single neuron activity, while ignoring population information embedded in the microscopic recordings. The biophysical basis underlying intracellular processes has been described especially thoroughly (for an overview: Koch and Segev, 2000).

Since the emergence of microelectrodes (Adrian and Zotterman, 1926), extracellular spiking activity has been used extensively to study neural correlates of behavior and sensory processing in vivo (Adrian and Moruzzi, 1939; Hubel and Wiesel, 1962). These spike trains can typically be detected in the high-frequency spectrum of the extracellular field potential, EFP (∼>500 Hz) (Logothetis et al., 2001). The low-frequency part (∼<300 Hz) of the EFP (Nunez, 2006), the local field potential (LFP), received less attention because of the complexity of interpreting its neuronal origin. The denomination "local field potential" actually is a misnomer, because it merely designates a local electric field. This field typically can be measured from the scalp (by EEG and magnetoencephalography, MEG), with intracranial or epicortical, non-penetrating disk electrodes (electrocorticogram, ECoG) or using intracortical penetrating electrodes (local field potential, LFP). Although these methods all sample from the same electric field, the latter will be called LFP as the terminology is generally used this way.

Recently, the amount of research in LFPs has increased significantly due to the possibility of measuring high-density signals across layers with multicontact electrodes (Barth and Di, 1991; Du et al., 2011). The LFP is thought to be composed mainly of summated synaptic currents emerging during synchronized cortical excitation (Mitzdorf, 1985; Eccles, 1951; Nunez, 2006), which contains information outside the scope of single unit recordings. Therefore, measuring at the scale of neuronal networks is of great importance, regarding the highly interconnected structure of the brain (Cajal, 1904; Friston, 1994). For example, cortical pyramidal cells are covered by approximately 10^4 to 10^5 synapses, from which ∼75% produce excitatory postsynaptic potentials (Abeles, 1991; Nunez, 2006). Using intracellular responses, Douglas and Martin (1991) demonstrated the importance of brain connectivity with a microcircuit which simulates experimental data. In other studies LFPs were used to determine network characteristics of properties such as motor control (Sanes and Donoghue, 1993; Heldman et al., 2006), sensory processing (Di et al., 1990; Einevoll et al., 2007) and memory (Pesaran et al., 2002; Liebe et al., 2012).

Due to the complex configuration of the charges generated by neuronal processes in the highly inhomogeneous extracellular space, the biophysical mechanisms underlying the genesis of LFPs are difficult to interpret (Nunez, 2006). In order to differentiate neuronal contributions to the LFP, many computational models have been developed (Einevoll et al., 2013). Typically, two types of modeling can be distinguished, forward-modeling and inverse-modeling. The first kind is used to model the EFP from transmembrane currents while the latter allows one to approximate the cortical currents based on the measured EFP.
A different, regularly used approach to decipher the EFP is converting the signal into the frequency domain using a Fourier transformation (Nunez, 2006). In the frequency domain different quantitative approaches can be used, such as co-variation within frequency bands and correlation with single unit recordings (Nielsen et al., 2006).

ECoG is a useful and widely used methodology to monitor neuronal EFPs at a global level with limited neuronal invasiveness (compared with intracortical recordings), making it especially suitable for research involving humans. The ECoG signal samples from a larger region than the LFP as it typically uses electrodes with smaller impedance (Toda et al., 2011). Furthermore, the cortical surface potentials have higher spatial resolution and signal-to-noise ratio than EEG. Under experimental conditions, for instance, certain low frequencies fluctuate with location in ECoG recordings but seem to be invariable in EEG measurements (Crone et al., 1998). Particularly flexible high-density multichannel electrode arrays can yield precise measurements (Takeuchi et al., 2005; Toda et al., 2011), even at a submillimeter spatial resolution (Viventi et al., 2010). Approximately a decade ago ECoG was introduced as a promising electrophysiological measurement to steer neuroprosthetic devices (Leuthardt et al., 2004; Ramsey et al., 2014). The electrodes can be implanted for long-term use because the risk of damaging the cortical tissue is limited (the cortical surface is usually not penetrated), resulting in durable and stable recordings (Chao et al., 2010). The high signal fidelity renders ECoG well suited to decode motor- or sensory information used for efficient brainmachine interfaces (BMIs) (Schwartz et al., 2006).

Understanding the underlying activity and limitations of the signal ECoG samples from is necessary to design BMIs effectively and for highly accurate functional mapping before resection. This review will discuss factors involved in the generation of the EFP through several approaches, such as describing the neuronal architecture and electrical properties of neuronal tissue. The main focus will be computational models and types of analyses which arguably are essential to disambiguate underlying neuronal contributors. Generally, modeling and functional frequency decoding studies address intracortically measured EFPs, using LFP recordings. Here, an attempt will be made to combine this literature with that concerning

intracranially sampled EFPs, ECoG. In order better to understand physiological measures of neural activity, the mathematical relation between neuronal dynamics and different experimental modalities must be studied (Deco et al., 2008; Logothetis, 2002).

2. Factors in the generation of the EFP

Any type of transmembrane current (e.g., created by excitable membranes such as spines, dendrites, axonal nodes of Ranvier, soma of the neuron) contributes to an electric field potential, the EFP. All these ionic processes in the brain superimpose an electric field, which can be measured as V_e at a certain location, both intracellularly and extracellularly. This superposition principle (the net response caused by multiple stimuli is the sum of these responses) is an important property of linear systems, rendering mathematical methods such as Fourier and Laplace transformations applicable. The measured waveform characteristics of the EFP (such as frequency composition, sign and shape) depend on the numerous contributing sources and properties of the brain tissue the current travels through. The spatial density, polarity and magnitude of the individual sources as well as the temporal coordination of these current sources (synchronization of neuronal activity) determine the shape of the extracellular field. These key shaping factors (the neuronal architecture, geometry and temporal synchrony of neural networks and the contributions of the individual neuronal activities) will be discussed in more detail below.

2.1. Individual contributors to the EFP

Synaptic activity.

Synaptic activity is generally regarded as the dominant component of cortical EFPs. For extracellular currents to induce a measurable signal, currents from many individual sources must coincide. And this overlap in time is more likely to occur with slow processes like synaptic currents (Mitzdorf, 1985; Logothetis and Wandell, 2004; Nunez, 2006).

Extracellular sinks typically emerge when neurotransmitters act on synaptic NMDA (Ca^{2+} and Na^+ influx) and AMPA (Na^+ influx) receptors, causing cations to flow into the synapse. Because of the principle of charge conservation (the total charge entering and leaving equals zero across the entire membrane of the cell) there is a passive ionic current from intracellular to extracellular space. Ruled by the electroneutrality principle, a return current (an extracellular source) is formed to maintain the equilibrium between cations and anions. A sink is defined as a flow of positive charge away from the recording electrode or a flow of negative charge toward the electrode. Vice versa, a source is a flow of positive charge towards the electrode or a flow of negative charge away from the electrode. Thus, when measuring intracellularly, the example with NMDA receptors would produce a source.

Similarly, inhibitory currents mediated by GABA subtype B ($GABA_B$) and GABA subtype A ($GABA_A$) receptors stimulate the opening of K^+ and Cl^- channels causing an efflux of cations or influx of anions, respectively. However, $GABA_A$ receptor induced currents contribute minimally to the extracellular field because the resting membrane potential and the equilibrium potential of Cl^- are almost the same (Woodin et al., 2003; Purves et al., 2004). There can be a $GABA_A$ effect when neurons are spiking, because the membrane will be depolarized and then the inhibitory Cl^- can generate measurable transmembrane currents (Glickfeld et al., 2009; Bazelot et al., 2010).

Depending on the sink-source configuration, a dipole or higher order pole emerges (Nunez, 2006; Lindén et al., 2010). This will be discussed in more detail in Sections 2.2 and 3.1.

Spiking activity.

Action potentials occur due to an increased permeability of the neuronal membrane to Na^+ generating a strong current, which can be measured as spiking activity. The amplitude of a spike typically decreases exponentially as the distance from the soma increases. In contrast to synaptic signaling, the short duration of the spike generated electric fields (less than 2 ms) implies that not many contiguous neurons are likely to fire synchronously in this limited timescale. Therefore, until recently these large local V_e deflections were thought to make only a minimal contribution to the EFP frequency spectrum. However, synchronous and frequent spiking activity of a population of neurons could contribute to specific frequency bands of the EFP, mainly in the high-frequency spectrum (Niedermeyer and da Silva, 2005; Ray and Maunsell, 2010).

More complex dendritic spikes can make major contributions to the EFP as well, because voltage-dependent Ca^{2+} channels give rise to slow Ca^{2+} mediated spikes (Wong et al., 1979; Golding et al., 1999). However, distinguishing Ca^{2+} spikes from excitatory postsynaptic potentials (EPSPs) is complicated since both can be induced by NMDA receptors (Schiller et al., 2000; Larkum et al., 2009). Buzsaki et al. (1996) recorded dendritic Ca^{2+} spikes extracellularly from a CA1 pyramidal cell (Figure 1A-E). They observed that weak commissural stimulation (B-C), indicated by arrows and lower trace, can delay (B) or even abolish (C) the slow, large Ca^{2+} spike. If the Ca^{2+} spike occurs before the arrival of the dendritic current injection, it is aborted (D) and when the magnitude of the stimulation increases (E), a decay of fast-spike amplitude is measured. Another study (Helmchen et al., 1999) measure dendritic Ca^{2+} spikes with a complex recording configuration, simultaneously performing calcium imaging and recording intracellular recording and ECoG (Figure 1F). These slow Ca^{2+} spikes exhibit a temporal signature within the low-frequency spectrum, comparable with synaptic currents. The dendritic depolarization is approximated with a smoothed spike curve (G, left). The integral of the smoothed dendritic curve describes the amount of current flow and this integral curve resembles the Calcium Green-I's fluorescence trace (G, the two upper right traces). The derivative of the curve has a close resemblance to the recorded ECoG spike (G, the two lower right traces). Figure 1H illustrates the relation between various dendritic depolarization amplitudes (arrows) and the Ca^{2+} flux. Finally, the recorded ECoG spike potential is correlated with intradendritically measured potential (I).
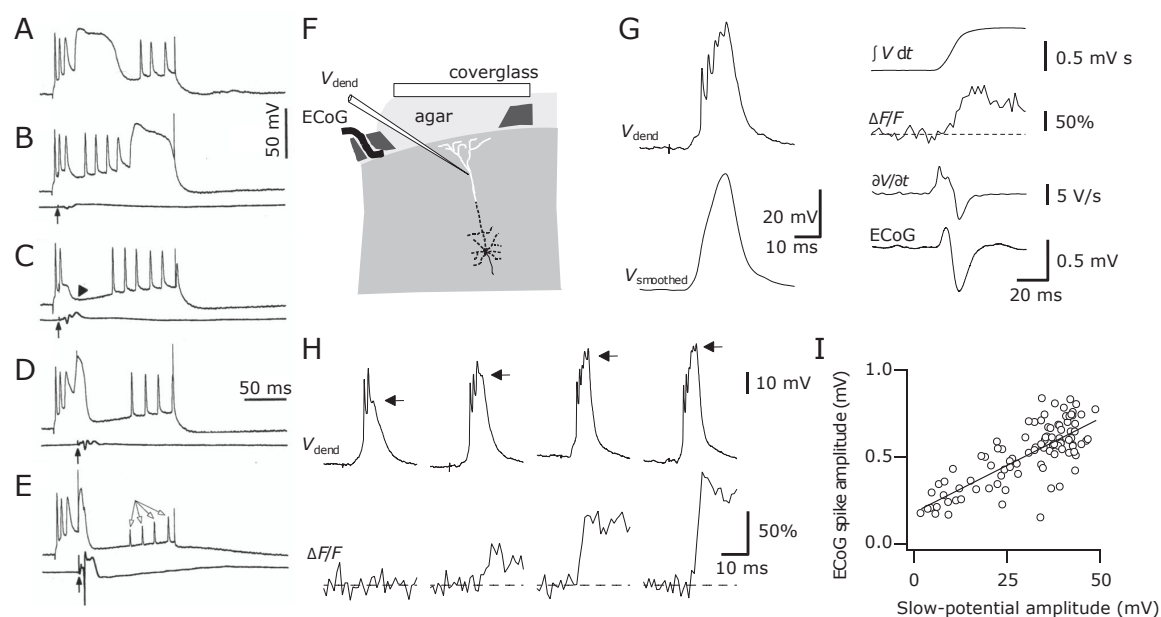

Figure 1: (A) illustrates an extracellular Ca^{2+} spike recording from a CA1 pyramidal neuron. Weak commissural stimulation (lower traces) delayed (B), abolished (C) or aborted (D) the dendritic spike. An increased stimulation (E) reveals a diminished amplitude of late fast spikes. (F) Depiction of the recording configuration with intracellular recordings having a resistance of 70-150 MΩ and ECoG being sampled at 0.1-300 Hz. The craniotomy was filled with agar to minimize motion and overlaid with a coverglass. Electrodes containing the Ca^{2+} indicator Calcium Green-I were inserted through the agar. (G) Left traces depict the intracellularly recorded dendritic spike and the curve after smoothing. The two upper right traces show the integral of the smoothed dendritic spike curve and the similar looking Ca^{2+} fluorescence recording. Bottom traces display the derivative of the smoothed curve and below it the recorded ECoG spike, which has a close resemblance to the derivative. (H) Several dendritic spike amplitudes and their relation to the Ca^{2+} flux. (I) Dendritic spike amplitudes recorded with ECoG depicted against the dendritic depolarizations display a positive correlation with r=0.82. A-E reproduced from Buzsaki et al., 1996 and F-I from Helmchen et al., 1999

Finally, the afterhyperpolarization (AHP) occurring after action potentials may contribute significantly to the EFP (Buzsáki et al., 2012). Different types of AHPs can be distinguished: fast and medium AHPs mediated by high-conductance Ca^{2+} activated K^+ channels (brief duration) and slow low-conductance Ca^{2+} activated K^+ channel regulated AHPs (lasting from hundreds of microseconds to seconds) (Bean, 2007). While fast and medium AHPs can be generated by a single action potential, slow AHPs typically emerge

when multiple spikes occur. So AHPs induced by Na^+ and Ca^{2+} spikes can contribute to the EFP because they have a magnitude and duration comparable to that of synaptic processes (Buzsáki et al., 1988). For instance, AHPs might mediate the EFP shifts observed during movement preparation (Kornhuber et al., 1969; Christie and Kamen, 2010).

Contributions of action potentials to the EFP will be addressed in 4.5 using a forward-modeling scheme.

Indirect EFP contributors.

Gap junctions allow the transmission of ions and various molecules between cells. While gap junctions themselves do not directly contribute to the extracellular current, they do affect excitability by facilitating ionic flow between neurons and thus can increase neuronal synchronization (Barth, 2003).

A study by Kang et al. (1998) shows that glial cells can noticeably affect the EFP. They demonstrated an astrocyte-mediated inhibitory synaptic transmission between hippocampal pyramidal neurons and interneurons. A recent modeling study describes how astrocytes may move cations from the extracellular space after neuronal activation (Halnes et al., 2013). Their model incorporates several processes of astrocytes that influence the movement of ions, such as axial transport and the location where cations are released. Neuron-glia interactions have been proposed in several studies to contribute to slow field patterns (<0.1 Hz) (Petsche et al., 1984; He et al., 2008; Kang et al., 1998).

Ephaptic coupling.

Due to the conductive nature of the extracellular medium, electric fields cause changes in the transmembrane potential of neurons (Chan and Nicholson, 1986; Anastassiou et al., 2011, 2010; Radman et al., 2007). Arvanitaki (1942) introduced the term 'ephapse' ('to touch') to describe the interactions between neighboring (touching) neuronal cells and electrical currents. Ephaptic coupling might increase synchronization in both inhibitory and excitatory neuronal activity, for instance during hippocampal theta waves (Jefferys, 1995; Anastassiou et al., 2011). The effect of LFP induced ephaptic changes on single neurons might be necessary to accurately model the LFP signal (Bédard and Destexhe, 2009 and discussed further in 4.4.2).

2.2. Cytoarchitecture

To understand the relative contributions of the various ionic currents influencing the EFP, the architecture of the cortical tissue and the shape of individual neurons need to be addressed. First, Lorente (1947) introduced open- and closed-field models to compute the EFP during an action potential. The geometrical configuration giving rise to a closed field is a sink or source at minimum separation from the return current, which keeps the potential and currents generated within a confined region. For example, the EFPs and currents remain confined within the architecture of the hippocampus, being folded onto itself, and thus the hippocampal field signature approximates a closed-field arrangement. Furthermore, in the human hippocampus the pyramidal cells are not neatly aligned and occupy numerous rows, so the potential is canceled out by the source and sink currents flowing in opposite directions. Cells with symmetric dendritic branching, i.e. stellate cells (Rall, 1962), anatomically imply a closed-field configuration as well. Theoretically a symmetrical synaptic input pattern would cause a closed-field configuration, since the various nearby contributions cancel out. However, this will only occur if sufficient synaptic inputs occur equally spaced around the dendritic arborization. Therefore, even though the morphology suggests a closed-field, stellate cells can contribute significantly to the EFP (Figure 2).

Pyramidal cells are the most ubiquitous neuron type in the neocortex, with distinct dendritic trees at the base (basal dendrites) and at the apex (apical dendrites) of the soma. The long dendrites of pyramidal neurons create a geometrical configuration with substantial space between sink and source. This results in a considerable ionic flow which contributes substantially to the EFP. Because of the large number of pyramidal cells and their spatial alignment they give rise to the majority of the generated cortical dipole moments. Therefore, the cerebral cortex could be viewed as an open-field configuration (Rall, 1962).
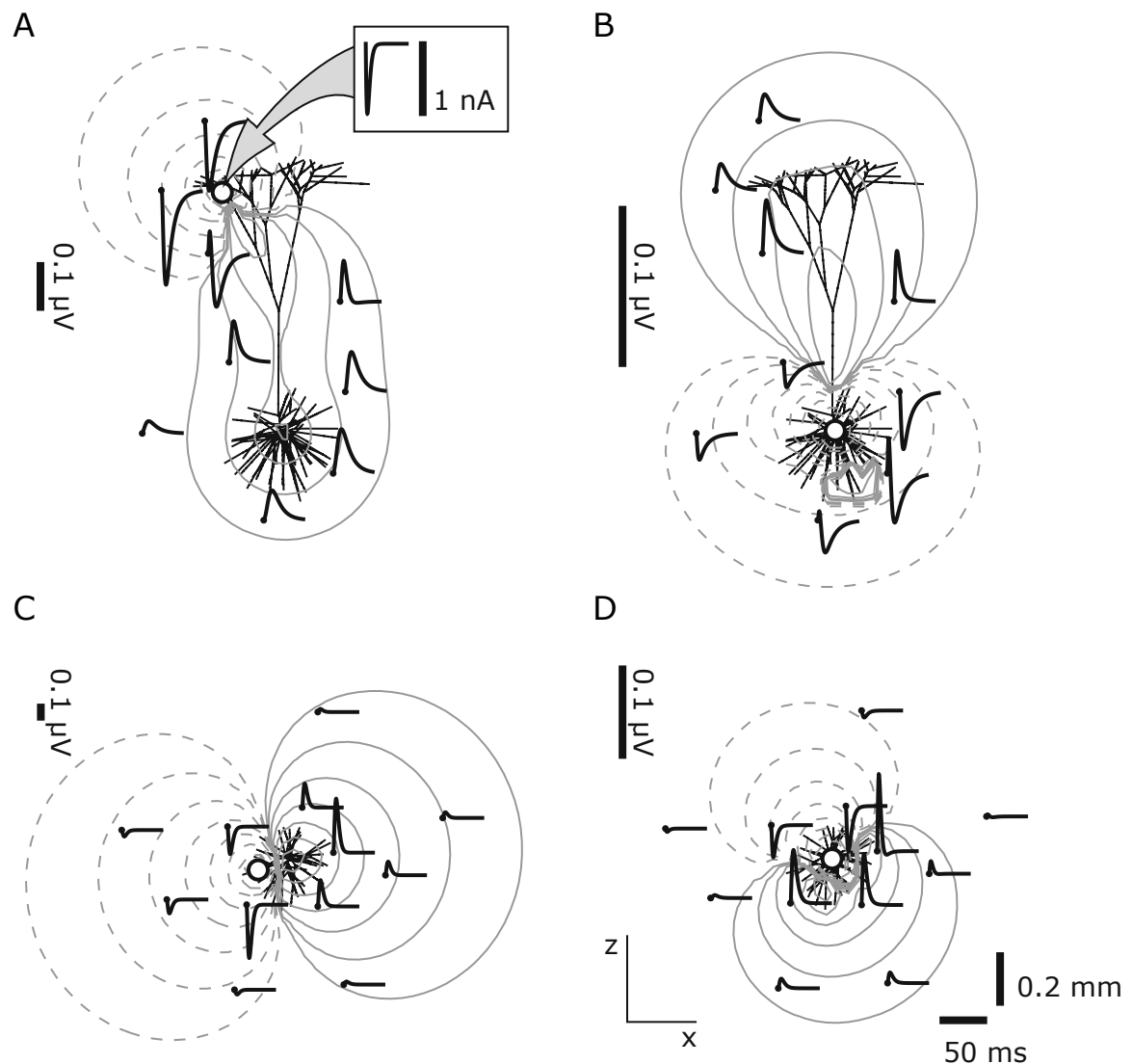
Figure 2: Several LFPs generated with a passive neuron model (i.e. there are no active dendritic ion channels, values of electric parameters can be found in Lindén et al.) from the cat visual cortex receiving input from one excitatory synapse (white circle, a negative current is injected described by an α-function, displayed in A). This illustrates how different dendritic arborizations, locations of the active synapse and positioning of the recording electrode affect the LFP. The LFP induced by an EPSP at apical dendrites and at the soma of a simulated layer 5 pyramidal cell (A and B, respectively) and at distal dendrites and at the soma of a simulated layer 4 stellate cell (C and D, respectively). The LFP of each cell is displayed at specific locations around the neuron (the black dots indicate the location, the black line emerging from it displays the LFP at that particular position). The solid gray contour lines enclose the positive LFPs and the dotted contour lines the negative LFPs. The contour traces are spaced logarithmically illustrating the amplitude decays by factor 2, the expected dipole decay rate. Reproduced from Lindén et al., 2010

The magnitude of the EFP is inversely proportional to the size of the brain (Kahana et al., 2001; Csicsvari et al., 2003; Buzsáki et al., 2003), with mouse > rat > cat > primate. Perhaps this can be attributed to a smaller amount of rows resulting in less cancellation of non-aligned neurons. Further, pyramidal neurons are less closely packed in large brains than in small mammalian brains (Herculano-Houzel et al., 2007). The result is a higher conductivity (considering the cell membranes' capacitance) and thus neurons are more likely to cancel each other out. The folded geometry of the cortex (in mammals having a sufficiently large cortex, that is) is a third factor influencing the magnitude of the EFP (Niedermeyer and da Silva, 2005). Dendrites are packed more densely at the concave side (the sulcus) than at the convex side of a gyrus which causes differences in the current densities (Buzsáki et al., 2012).

6

2.3. Temporal synchrony

The magnitude of the EFP cannot be explained solely by structural properties of the cortex, synchrony of neural networks is another important factor. Neural networks are oscillatory systems in which single cells are the oscillators. One definition of synchrony is the temporal coherence of firing rates. For example, coupled neural inputs would result in synchronization. Another, stricter, definition of synchronization is a phase relation (in-phase, anti-phase or involving some kind of phase-shift) or the exact concurrence of neural events. Neurons can be coupled through electrical and chemical synapses (Kopell and Ermentrout, 2004). Gap junctions (which influence electrotonic communication between neurons) have for instance been discussed in connection with synchronized bursts and epileptic seizures (Perez Velazquez and Carlen, 2000).

Quantifying synchronous oscillations of neural potentials can be done by cross-correlating the membrane potential fluctuations of a population of neurons over a large amount of time (Hansel and Sompolinsky, 1996). Several other methods have been used to calculate the amount of synchronization as well, e.g. mutual information, phase synchronization, non-linear interdependence (for a comparison, Kreuz et al., 2007). As expected, the magnitude of electric potentials increases in proportion to the neuronal synchrony (figure 3). Lindén et al. (2010) demonstrate that synchronized synaptic sources (created by correlated synaptic input) generate a stronger LFP with a larger spatial spread compared with uncorrelated input trains. (More about spatial spread and its implications for synchrony in Section 4.2).
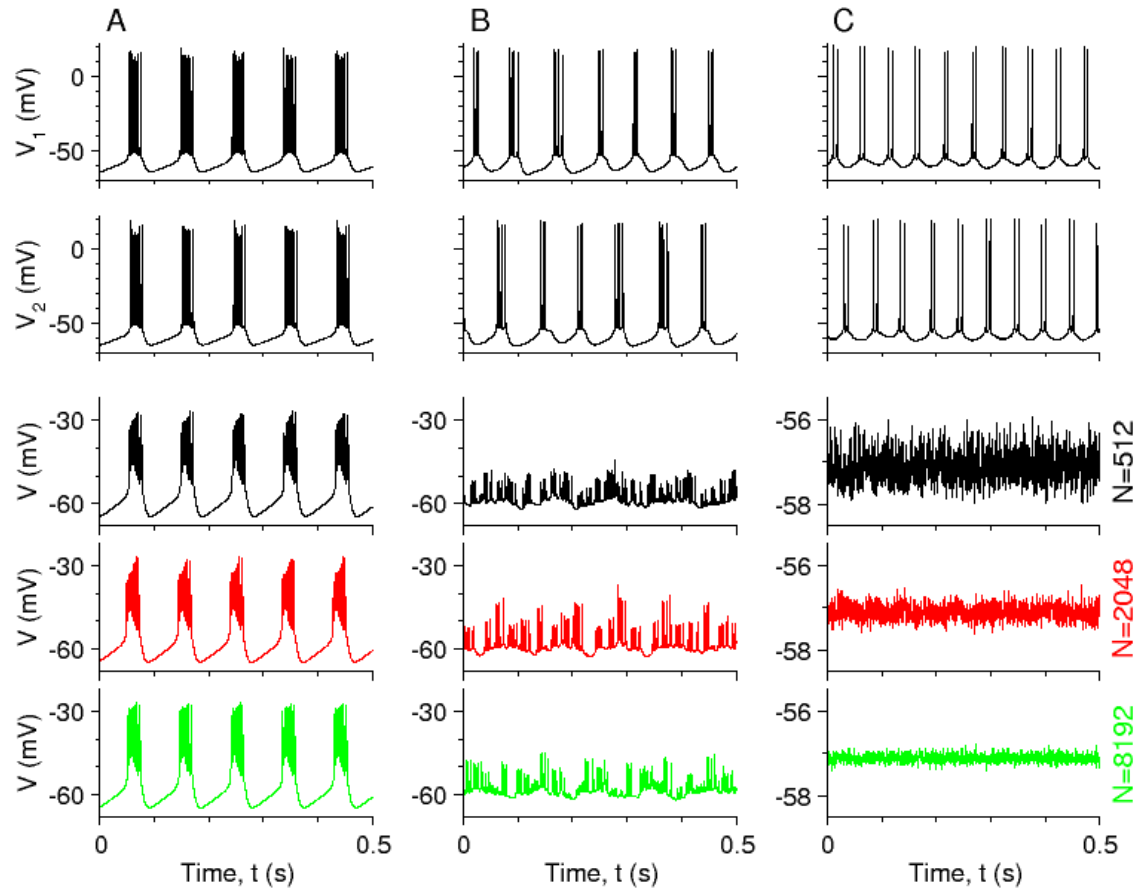

Figure 3: Simulated neuronal bursting patterns with (A) high synchrony, (B) low synchrony, (C) no synchrony. The upper two graphs of each column display the electric potential of two single neurons from the population containing N = 512 neurons. The lower three panels show an attenuation of the fluctuations in (C) with populations of 512, 2048, 8192 neurons, while the amplitude remains constant in (A) and (B). When $N \rightarrow \infty$ the amplitude of the asynchronous bursts will approximate zero. The connectivity of the model is described by each neuron being connected to every other neuron. Reproduced from (Golomb, 2007)

3. Basic modeling schemes

3.1. Forward-modeling the EFP

An electric field exerts a force on charged particles and can be transmitted through biological tissue, i.e. by volume conduction. Volume conductor theory describes how volume current sources (transmembrane currents) propagate through biological tissues towards a recording site (Ebersole and Pedley, 2003; Lindén et al., 2010). Depending on the spatial configuration of sink and source a dipole or higher order pole can be formed. Notably, at the scale of the membrane sinks and sources are distributed along its surface without a current flow between two poles. At larger distances however, (approximately four times the diameter of the sink-source axis) the potential will display a signal as if produced by a dipolar current flow (dipole approximation). For cortical EFPs, volume conduction modeling studies demonstrate that contributions from synaptic inputs seem to be the biggest component in generating dipole moments (Einevoll et al., 2007; Pettersen et al., 2008). The EFP's biophysical origin is well understood in the framework of volume conductor theory (Nunez, 2006) and forward-modeling based on multicompartmental neuron models has been widely used (Rall and Shepherd, 1968; Destexhe, 1998; Holt and Koch, 1999; Gold et al., 2006; Pettersen and Einevoll, 2008; Lindén et al., 2010, 2011). Indeed, the fact that electrical recording methods such as EEG and ECoG are possible robustly demonstrates the extent of volume conduction (Buzsáki et al., 2012).

Cortical tissue consists of tightly packed neurons embedded in a low-resistance extracellular medium (Nunez, 2006; Brette and Destexhe, 2012). In this biophysical framework the relation describing the extracellular potential $\phi(t)$ measured at electrode position r_e caused by a transmembrane current $I_0(t)$ at position r_0 may be described as follows:

$$\phi(r, t) = \frac{1}{4\pi\sigma} \frac{I_0(t)}{|r_e - r_0|} \tag{1}$$

Basically, this equation describes how the contribution of one point source in an isotropic volume conductor is inversely related to its distance from the electrode (Figure 4). The extracellular conductivity σ is the reciprocal of the resistivity and describes the ease with which ions can pass through extracellular tissue. According to this formalism, at an infinitely faraway point from the transmembrane current the extracellular potential is zero. The point-source equation of the current flow relies on the assumption that there is a point from which the membrane currents emanate (Holt and Koch, 1999). Conceptually, this point-source approximation is sufficient to explain EFPs generated by any transmembrane current. A different, frequently used approach to describe transmembrane currents is the line-source approximation (Holt and Koch, 1999; Pettersen et al., 2008). To obtain the EFP generated by a line-source, Eq. 1 is expanded with a function of the geometric distances of the segment with the assumption of evenly distributed currents.

The above formula relies on a set of assumptions (described in detail in Brette and Destexhe, 2012). Among these assumptions is the quasistatic approximation obtained from Maxwell's equations (neglecting the time derivatives of the electric and magnetic field equations and thus leaving them effectively decoupled). Also the extracellular conductivity and permittivity (ϵ) should be isotropic (i.e. the same in all directions), frequency-independent (i.e. not variable with frequency) and homogeneous (uniform throughout the extracellular medium). Assuming this for σ and ϵ is equivalent to assuming a purely resistive medium, such as salted water. If the assumptions are violated adjustments are possible; anisotropic conductivity, for instance, could easily be incorporated in the formula by replacing the denominator with $4\pi\sqrt{\sigma_y\sigma_z(x - x_0)^2 + \sigma_x\sigma_z(y - y_0)^2 + \sigma_x\sigma_y(z - z_0)^2}$ (Nicholson and Freeman, 1975). Solving violations to the frequency-independence assumption is discussed in Section 4.4.1.

While Eq. 1 applies to single transmembrane currents, we can easily generalize it to many transmembrane current sources. Using the principle of linear superposition provides us with a multicompartmental formula with N point sources:

$$\phi(r, t) = \frac{1}{4\pi\sigma} \sum_{n=1}^{N} \frac{I_n(t)}{|r_e - r_n|} \tag{2}$$

A schematic representation of the multicompartmental model is illustrated in Figure 4. It is important to take notion of Kirchhoff's current conservation law when calculating EFPs due to neuronal activity.

Kirchhoff's current law states that the net transmembrane current coming out of a neuron has to add up to zero. Thus, in the multicompartmental neuronal model with N compartments $\sum_{n=1}^{N} I_n(t) = 0$ should apply. This would also imply that one-compartment models do not generate an EFP because the transmembrane current has to be zero. To produce an EFP, the simplest model consists of two compartments forming a dipole (Einevoll et al., 2013). The electric potential of a dipole decreases as $1/r^2$, whereas for a monopole this is only $1/r$. Dipoles decay faster due to the summation of the opposing charges of the sink and source. Similarly, higher order poles attenuate at an even higher rate because of the charges canceling each other out. Recent studies (Bédard and Destexhe, 2011; Destexhe et al., 2012; Riera et al., 2012) indicated that monopoles could exist at a population scale. They even suggest that monopoles reflect the ionic current at the scale of single neurons. However, this is not in agreement with many electrophysiological models (Gratiy et al., 2013), e.g. the well funded Hodgkin-Huxley model which describes the electrical characteristics of excitable neurons (Hodgkin et al., 1952). Gratiy et al. (2013) discuss several other explanations for the monopolar current sources. However, this subject is still under debate. Note that, although dipoles seem an intuitive representation of synaptic transmembrane currents, multipolar configurations can be composed of an arrangement of monopoles (Purcell and Morin, 2013).
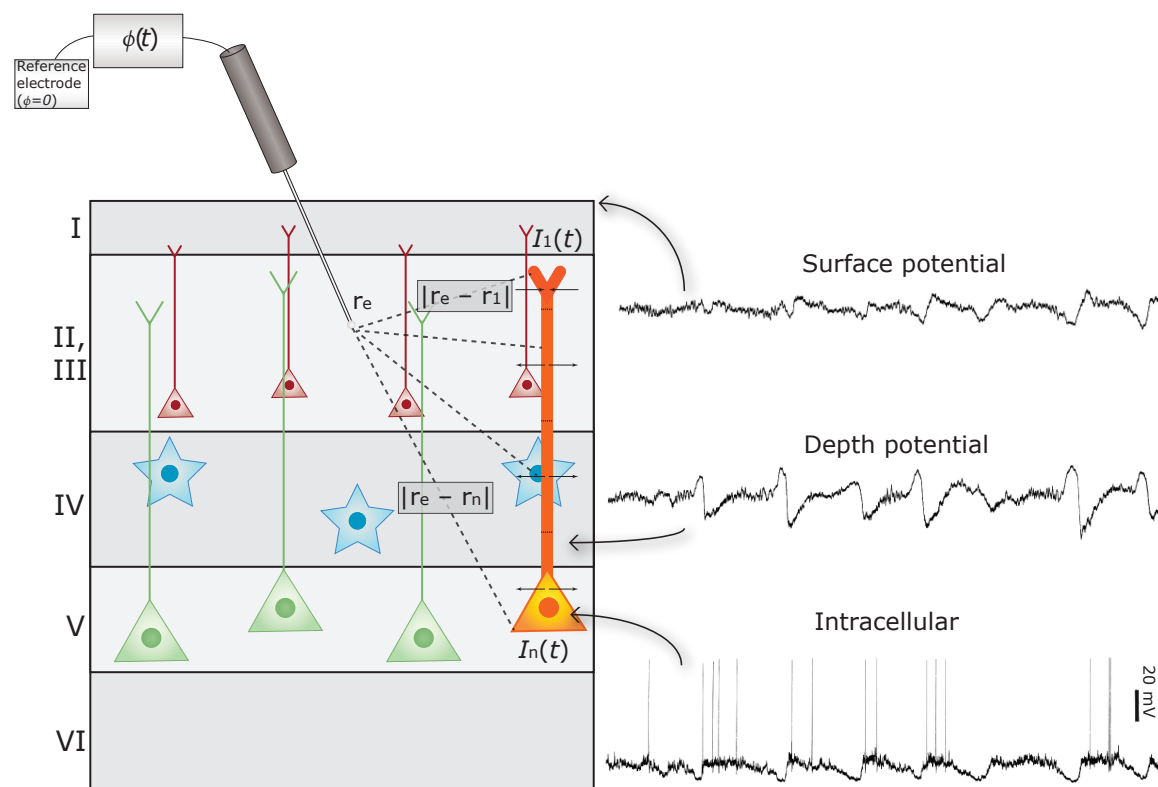

Figure 4: A schematic representation of the layered cortical structure containing stellate cells (blue), different sized pyramidal cells (layer-3, red and layer-5, green) and the signal recorded at different locations. The orange pyramidal cell receives excitatory input at its apical dendrite creating a tranmembrane current sink and a number of comparments with return currents (creating an extracellular source). This illustrates the multicompartmental point-source model with n segments and their respective current amplitude and direction (displayed by the arrows). Recorded oscillations reproduced from Contreras and Steriade, 1995

In order to make a numerical calculation of the EFP, on must first simulate a neuron and its transmembrane currents. Multicompartmental neurons are usually simulated with tools such NEURON (Carnevale and Hines, 2006) and GENESIS (Bower and Beeman, 1995). Then, Eq. 2 is used to calculate the EFP on the basis of the spatial configuration of the simulated neuron and its ionic currents. This way the forward-modeling scheme can be used to describe characteristics of the LFP by varying multiple factors such as dendritic morphology, synapse location and input synchrony (Rall and Shepherd, 1968; Holt and Koch,

1999; Lindén et al., 2010), which provides insight into the underlying neuronal activity of recorded potentials. For instance, Lindén et al. (2010) models excitation at several dendritic branches of a reconstructed layer 5 pyramidal neuron and of a reconstructed layer 4 stellate cell (Figure 2). Besides the apparent decrease in amplitude with increased distance from the neuron, the shape of the LFP seems to broaden (an increased half-width of the potential, addressed in further detail in Section 4.3). This frequency-dependent behavior of the signal is an important reason why action potentials are less prominent in the LFP. Frequency scaling of the LFP will be discussed further in Section 4.3. The size and sign of the amplitudes in (Figure 2A) display positive LFPs near the soma (indicating sources because of return currents) with rather high magnitudes (illustrating non-linear decay, regarding the distance of ~1 mm from the current injection).

Another example applies the forward-modeling scheme to describe spike-and-wave epileptic seizures (Destexhe, 1998). Several types of epilepsy display absence seizures with typical spike-and-wave patterns in the ECoG and EEG signal (Jasper and Kershman, 1941; Destexhe, 1998; Cortez et al., 2004). The generation of these spike-and-wave patterns has been related to synchronous cortical firing (spike) and receptor-mediated responses (wave) in thalamocortical radiations (Steriade and Contreras, 1998). Destexhe (1998) simulates the spike-and-wave patterns using Eq. 2 while incorporating synaptic currents, the forward-generated LFP, intrinsic membrane currents and thalamocortical connectivity. The spike-and-wave pattern was simulated with synchronous postsynaptic potentials (that generated the spike) and thalamic $GABA_B$-mediated inhibition (giving rise to slow K^+ currents).

3.2. Inverse-modeling the EFP

The forward-modeling equation discussed previously estimates the EFP on the basis of neuronal activity. A related approach attempts the opposite, estimating the activity in neurons from the EFP, which causes the inverse problem (Tarantola, 2005; Nunez, 2006) because macroscopic variables are used to infer microscopic ones. For the LFP this means estimating current sources and sinks from the recorded volume-conducted electrical field. The common approach to a solution of the inverse problem is solving the forward formula (Eq. 2) first. To this end, constraints must be added (Leski et al., 2011; Nicholson and Freeman, 1975). First, the relation between microscopic and macroscopic events must be described (Mitzdorf, 1985; Buzsáki et al., 1986; Einevoll et al., 2007). Second, it should be possible to model LFPs from its components (e.g. synaptic currents) experimentally (Buzsáki et al., 2012). Generally, current source density (CSD) analysis is used to quantify the amount of current displacement in the extracellular medium (Nicholson and Freeman, 1975; Mitzdorf, 1985). Conceptually, the CSD estimates currents at a spatial resolution of tens of μm; however, because of the inter-contact distance this is rather in the order of hundreds of μms.

3.2.1. CSD analysis

CSD estimates typically use evenly spaced laminar multielectrode arrays inserted orthogonally into the cortex; they are a quantification of the volume density of the net current flow in the medium. Theoretically CSD analysis can be illustrated by considering a population of pyramidal neurons being excited by input at their basal dendrites. This results in a typical dipole (sink-source) CSD distribution, which can be measured as a field potential using a multielectrode. The difference in potential over extracellular space (using the evenly distributed contact sites of the laminar multielectrode) can be estimated as difference in potential per distance.

First, the relation between the electric potential and CSD is described as an integral, by reformulating Eq. 2:

$$\phi(r,t) = \frac{1}{4\pi\sigma} \int \int_D \int \frac{C(r',t)}{|r_e - r'|} d^3r' \tag{3}$$

This volume integral (in the Cartesian coordinate system) within region D integrates over the CSD C(r) (unit A/m^3) measured at the position of the electrode r_e. The quantity of the CSD is described by $C(r,t) \equiv \sum_{n=1}^{N} I_n(t)\delta^3(r - r_n)$ with δ^3 describing the 3-D Dirac delta function. The inverse algorithm of this equation is described by the Poisson equation. It can be obtained by combining (1) the relation between the electric

field E to the potential ϕ, $E = -\nabla\phi$ with (2) the current conservation described by the relation between the current density j and the electrical field $\nabla \cdot (\overrightarrow{\sigma} E + \overrightarrow{j}) = 0$ (Brette and Destexhe, 2012):

$$C(x, y, z) = -\sigma\left(\frac{\partial^2}{\partial x^2} + \frac{\partial^2}{\partial y^2} + \frac{\partial^2}{\partial z^2}\right)\phi(x, y, z) = -\sigma\nabla^2\phi(r, t) \tag{4}$$

This differential is valid when conductivity σ is isotropic (the same in all directions) and constant, but the formula can be adjusted (Brette and Destexhe, 2012) by for instance making the conductivity dependent on position ($\sigma = \sigma(r)$).

CSD analysis relies on the laminar architecture of the cortex and presumes variation to happen mostly in one directional plane (vertical variability across the laminae is assumed to be large compared with lateral variability). Based on this characteristic, a simplified version of the equation can be obtained, with a CSD estimate along only one axis (z), neglecting the other two planes (x,y) (Nicholson and Freeman, 1975):

$$C(z_j) = -\sigma\left(\frac{\phi(z_j + \delta) - 2\phi(z_j) + \phi(z_j - \delta)}{\delta^2}\right) \tag{5}$$

This estimate of the CSD can be quite erroneous, e.g. when the source diameter is small. Different approaches to compute the CSD have been introduced in 3-D (Nicholson and Freeman, 1975) or with the inverse CSD analysis, which makes use of the forward solution to take into account activity along the neuronal population activity (Leski et al., 2011; Pettersen et al., 2006; Leski et al., 2007). This method has been successfully validated by first forward-modeling the EFP and subsequently using the inverse CSD to test its accuracy at predicting the underlying activity (Pettersen et al., 2008).

Zhang et al. (2008) reconstruct current densities from subdural ECoG recordings using the finite element analysis (FEA). Their ECoG current density reconstruction transforms the Poisson equation into a set of linear equations along the FEA grid, describing the dipole moments along this grid. Their solution to the inverse problem may prove useful to localize the seizure focus of epilepsy patients.

4. Properties of the LFP

The LFP signal is particularly difficult to interpret compared with spiking activity due to the large amount of contributing sources, discussed previously. Early studies initially proposed that the recorded oscillations can be attributed to action potentials in a specific neuronal circuitry (Bishop, 1936). A contrasting explanation suggested that oscillatory processes of the membrane potential, rather than spiking activity, are involved in the genesis of EEG (Bremer, 1938, 1944; Moruzzi and Magoun, 1949). The theory that the LFP and EEG stem from synchronized summated synaptic activity was first coined by Eccles (1951); it is still the leading explanation. Indeed, its truth has been demonstrated in intracellular measurements (Creutzfeldt et al., 1966) and modeling studies (Nunez, 2006). In this section several properties of the LFP are described and biophysical models based on the previous formulas are used to simulate these features.

4.1. Frequency bands and the underlying neuronal activity

The LFP is generally decomposed into frequency bands by applying a Fourier transformation, i.e. delta (2-4 Hz), theta (4-8 Hz), alpha (8-12 Hz), beta (12-30 Hz), and gamma (30-150 Hz). This categorization is typically defined phenomenologically (frequency bands are related to certain physiological states) and thus rather arbitrary. A functional division of the frequency spectrum could be achieved by analyzing whether frequency bands carry independent information about experimental tasks. Subsequently these frequency bands might convey distinct information about the underlying neuronal activity. Note that this approach based on co-variation is dependent on the presented stimuli, which should be highly divergent in order to distinguish between the underlying contributors.

The dependency of frequency bands on the underlying neuronal activity is generally measured using signal- and noise correlations (Belitski et al., 2008). Signal correlation (e.g. with the Pearson product-moment correlation coefficient) quantifies the dependence of neural recordings on different experimental stimuli. Most experimental designs are based on this concept. Noise correlations compute the opposite by

quantifying the covariation across trials (for instance, the relation between LFP and spikes without a changing stimulus), instead of across experimental conditions used in the signal correlation. Analyzing the LFP frequency spectrum with this approach enabled researchers to show the relation between the information conveyed in LFPs and spikes (Belitski et al., 2008). They found a significant positive signal correlation between the high-γ band and spikes. Belitski et al. (2008) also found a positive signal correlation between pairs of γ range frequencies suggesting this range carries information about the stimulus. The noise correlation was positive for low frequencies (<24 Hz) between pairs of LFP frequencies, which suggests that this frequency range conveys stimulus independent information, for example diffuse neuromodulatory mechanisms. This method also revealed a dissociation between the information contained by low and high frequencies. Instead of using these spike-related features of the LFP, David et al. (2010) regard them as an artifact when using high impedance electrodes to record the LFP (comparable to removing muscle artifacts in EEG). High impedance electrodes can pick up spikes close to the electrode-tip and nearby synaptic potentials dominate the signal. In David et al. (2010) the action potential signature is decoupled from the LFP with linear filtering methods to obtain the information conveyed solely by the LFP.

Dissociating between functional frequency bands can prove difficult when the noise and signal correlations are overlapping in the information they convey. For example, the relation between the high-γ band and spikes has been demonstrated in numerous studies (Crone et al., 2011; Ray et al., 2008b). It has received considerable attention because the information in the high-frequency band of the LFP could provide a link between the mesoscopic-level ECoG/EEG and the microscopic-level spiking activity of neuronal assemblies. The dissociation between high-γ frequencies and typical (narrowband) γ oscillations is still unclear however (Ray and Maunsell, 2011). Although high-γ bands show correlations with spikes, they might also reflect high frequencies originating from rhythmic inhibition, similar to γ oscillations.

Optimization techniques prove to be an effective alternative approach to the functional separation of correlated frequency bands (Siegel and König, 2003; Magri et al., 2012). The optimization in Magri et al. (2012) encompasses separating the frequency bands in such a way that the information about the stimuli is maximized. Such optimum partitioning of the frequency spectrum provided boundaries between the high-γ band and γ band. Furthermore, lower frequencies were divided into stimulus-independent and stimulus-dependent bands.

Another approach which addresses the distinction between transient fluctuations (for instance due to spiking activity) and oscillatory functions (which is traditionally done by applying Fourier transformations) is the matching pursuit algorithm (Ray et al., 2008a). This algorithm decomposes the signal by iteratively matching the best fitting function (i.e. typically a family of Gabors); then after each iteration the function is subtracted from the signal, ultimately resulting in a set of functions describing the signal. This analysis demonstrated that the high-γ band of ECoG recordings consists mostly of transient functions, once more indicating a relation to spiking activity. A study using comparable methods found similar results measuring LFPs and spikes (Ray et al., 2008b).

Although measuring the field potential at different scales often yields similar characteristics (Steriade, 2003; Buzsáki et al., 2012, Figure 4), there are fundamental differences in interpreting the signal. Ray et al. (2008a) use Eq. 2 to simulate the current source distribution of ECoG experimental data. This allowed them to demonstrate an increase in the high-gamma band of the frequency spectrum related to firing rate and, especially, neural synchrony. However, several studies indicate that broadband changes (over the entire bandwidth) in the frequency power spectrum are correlated with action potential firing (Manning et al., 2009; Miller et al., 2009). Miller et al. (2009) use a simple simulation (based on Bedard et al., 2006b) demonstrating this characteristic. Simply convolving a Poisson-distributed spike train with a postsynaptic current can imitate broadband spectral changes based on the spiking activity.

A few studies simultaneously measure and correlate ECoG and LFPs to address their relation (Toda et al., 2011; Watanabe et al., 2012; Peyrache et al., 2012). Peyrache et al. (2012) record both ECoG and LFP signals using the same electrodes demonstrating similarities in slow delta waves during slow wave sleep. Watanabe et al. (2012) recorded LFPs and multichannel micro-ECoG simultaneously to compare and reconstruct LFPs from ECoG recordings in the primary motor cortex. They found that ECoG signals resemble the LFP at recording sites just below the ECoG electrode. As expected, as the distance (and thus depth of the LFP electrodes into the cortex) increases the similarities decrease. The ECoG and LFP signals show a high resemblance at the surface (minimal distance between the recording position), particularly the β frequency band displays a relatively high correlation between the two measurements. The resemblance

at high-γ frequencies rapidly attenuates with deeper intracortical recording sites.

LFPs where reconstructed from the ECoG signal by weighted summations of the ECoG signal. In contrast to the correlation between the different signals, this produces an accurate reconstruction of the LFP at bigger depths. At small distances from the ECoG electrode (less than 2 mm) a small correlation with the reconstructed signal is observed in the high-γ band. The β and δ band were reconstructed with high accuracy.

One cause of differences between epi- and intracortical recordings is the sampling of ECoG from a large population of neurons compared with the LFP, due to a lower impedance of the electrode (typically a few kΩ vs. several hundred kΩ to a few MΩ). Furthermore, the electrode size and spatial sampling density profoundly influence the signal, which results in differences in decoding performance (Mehring et al., 2004). Yet another influential difference concerns the farther proximity of the ECoG electrodes to the current sources (epicortical vs. intracortical recording site). Thus the ECoG signal could be considered the LFP transformed by a large layer of neural tissue.

Despite this extensive amount of experimental evidence relating frequency bands to cortical activity, the changes at a neuronal level remain vague. Since a greater distance between current dipoles and recording site was demonstrated to exhibit an attenuation in high frequencies both theoretically and experimentally (Einevoll et al., 2013; Brette and Destexhe, 2012), less invasive techniques should have lower sensitivity for high-frequency activation. Thus, measurements such as ECoG and EEG do not reveal the full frequency spectrum and the decrease in high frequencies may even cause interference resulting in a power increase in narrow-band frequencies (Crone et al., 2011).

4.2. Spatial reach of the LFP

Depending on the current dipole and the conductive medium, some electric field patterns remain relatively local while others can be recorded far away from the current source (Lindén et al., 2011; Kajikawa and Schroeder, 2011). However, no clear consensus has been established yet on the amount of spatial reach of LFP (the size of the region underlying the signal). Indeed, highly diverging results have been reported on the amount of cortical spread of the LFP signal. Some reports show a literal 'local' LFP reflecting neural processing in an approximate range of 200-400 μm around the recording electrode (Katzner et al., 2009; Xing et al., 2009). Here the spread of the evoked LFP even appeared to match the multi-unit activity (MUA) spread across the cortical surface. Many other estimates of the amount of cortical propagation have been proposed, showing a lateral spread of LFPs over distances of 600-1000 μm (Berens et al., 2008; Gail et al., 2003; Kruse and Eckhorn, 1996; Liu and Newsome, 2006), 2-3 mm (Logothetis et al., 2001; Mitzdorf,
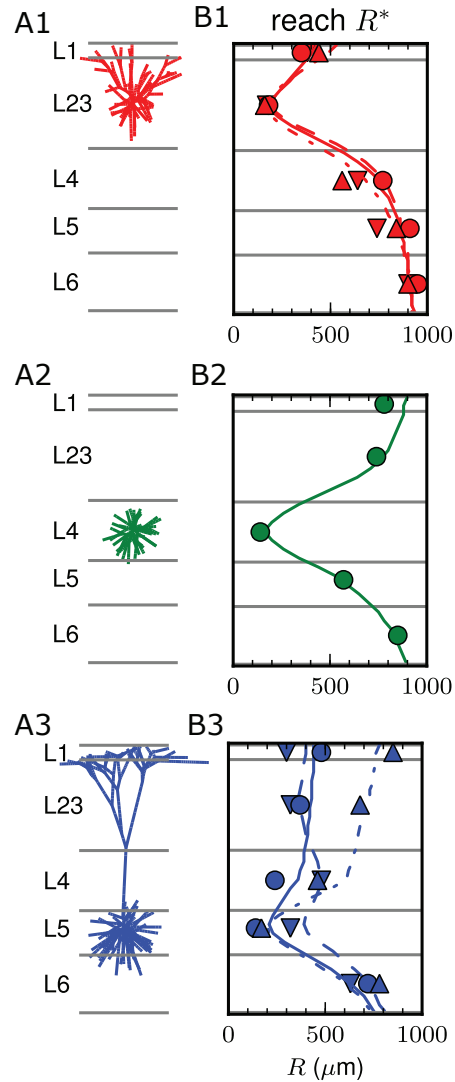

Figure 5: Populations of (A1) layer-3 pyramidal cell, (A2) layer-4 spiny stellate cell and (A3) layer-5 pyramidal cell receiving uncorrelated synaptic input. The radial reach R* (defined as the part of the neuronal population that contributes to 95% of the LFP amplitude) of the field potential along the layers for each cell type. Circles outline homogeneous synaptic input, triangles basal input and diamonds apical input. Only the layer-5 pyramidal cells display changes in the depth dependence of the population LFP with synaptic input location, the layer-3 cells seem largely independent of the synaptic distribution. Note that the LFP amplitude is largest at the soma, indicating a rather local LFP for these uncorrelated inputs. Reproduced from Lindén et al., 2011

1985; Nauhaus et al., 2008; Wang et al., 2005) and even up to 5 mm in Kajikawa and Schroeder (2011); Kreiman et al. (2006). However, comparing these studies is complicated because most use different stimulus conditions, measure different brain regions and do not even consider the same part of the LFP (e.g. evoked or induced potentials, frequency bands). Even two studies measuring LFPs in primary visual cortex (V1) using comparable approaches produced different estimates of the amount of cortical spread (Berens et al., 2008; Katzner et al., 2009).

Lindén et al. (2011) and Leski et al. (2013) simulated the size of the region of contributing neurons around an electrode and point out three factors that influence the spatial reach of the LFP which might reconcile the discrepancy between the previously mentioned studies. First, because of the superposition principle the contributions of all neurons in a population can be summated linearly, with neurons far from the electrode contributing less than neurons in its proximity. This involves describing how neuronal contributions attenuate as distance from the electrode increases. The second factor concerns the geometry and architecture of the neural population. Opposing the first factor, a typical disk shaped columnar population with evenly spaced neurons will result in linearly increasing amounts of neurons at a certain distance from the electrode as the distance increases. Finally, a key influence on the spatial reach of the LFP is the synchrony of the synaptic inputs contributing to the signal (resulting in correlated and thus amplified LFP contributors). This model predicts a spatial reach of approximately $200\,\mu$m for 95% of the LFP signal with uncorrelated synaptic activity (comparable with the findings of Katzner et al.; Xing et al.). Synchronized LFPs amplify the spatial reach and the signal could increase limitlessly combined with an increased population size.

This modeling approach could relatively easily be adjusted to model neural origin of the EFP measured with intraciranial electrodes (ECoG) or even at the scalp (EEG). The forward-model would have to incorporate the effects of the complex cortical tissue the electrical signal has to cross and, in the case of EEG, volume conduction along the scalp and skull (Nunez, 2006). One would expect the spatial reach of the signal to be larger because of the bigger electrodes with smaller impedance at a large distance from the neural currents. Although this was not directly addressed by Lindén et al. (2011), the LFP amplitude was modeled with different cell morphologies at their respective cortical layers dependent on electrode depth which can be used to predict ECoG estimations. The layer 1 electrode is comparable to ECoG measurements since it is close to the cortical surface and thus records a signal similar to the LFP (Watanabe et al., 2012). Their study shows that the spatial reach of the electrode at layer 1 is large compared with the soma layer for different cell morphologies (Figure 5). Combining this spatial spread with the type of electrode (which expectedly will sample from a larger region) might give an indication of the magnitude of the area ECoG samples from. It should be noted however that the simulation uses uncorrelated sources which is not representative for the generation of the ECoG signal.

4.3. Frequency scaling

As mentioned previously, the LFP shape gets broader as the distance from the current source increases. This is typically observed as a $1/f^n$ scaling of the power spectrum distribution and this power law can be observed in various other areas, such as seismology, finance and allometric scaling in animals (Stumpf and Porter, 2012). The power spectral density of both macroscopic (EEG) and microscopic (e.g. LFPs) measured transmembrane potentials display such power-law characteristics.

Figure 6 illustrates the dependence of the frequency power spectrum on the distance between the recording site and the current source. The power law of LFP describes a relation between the amplitude of the extracellular signal and its temporal frequency as a descending straight line on logarithmic scale that scales as $1/f^n$ (Milstein et al., 2009; Miller et al., 2009; Pritchard, 1992; Bédard and Destexhe, 2009). Various mechanisms have been suggested to underly the LFP frequency scaling, but its origin remains unclear. An intuitive explanation of the higher amplitude of low frequencies is the longer timeframe of lower frequencies, enabling more neurons to add to the potential. In Section 4.4 modeling studies will be discussed in which frequency scaling characteristics are simulated via the filtering properties of the conductive medium.

The simple way of modeling broadband changes used by Miller et al. (2009), discussed previously, indicates that the degree of power scaling $1/f^n$ is dependent on various factors such as the temporal shape of the rising and decaying of the postsynaptic current, synchronous firing and the dendritic configuration and therefore the type of neuronal cell (Milstein et al., 2009; Miller et al., 2009). The current influx and efflux generated transmembrane potential that is used is similar to the LFP (Okun et al., 2010) and likely

comparable with ECoG signals (Miller, 2010). Note that 1/f scaling is a phenomenological feature; so being able to simulate it does not necessarily mean that it describes the correct underlying neural activity causing it. And although this model is effective for describing experimental data (the power law scaling), it does not inform us about the generation and propagation of the electric field through cortical tissue.
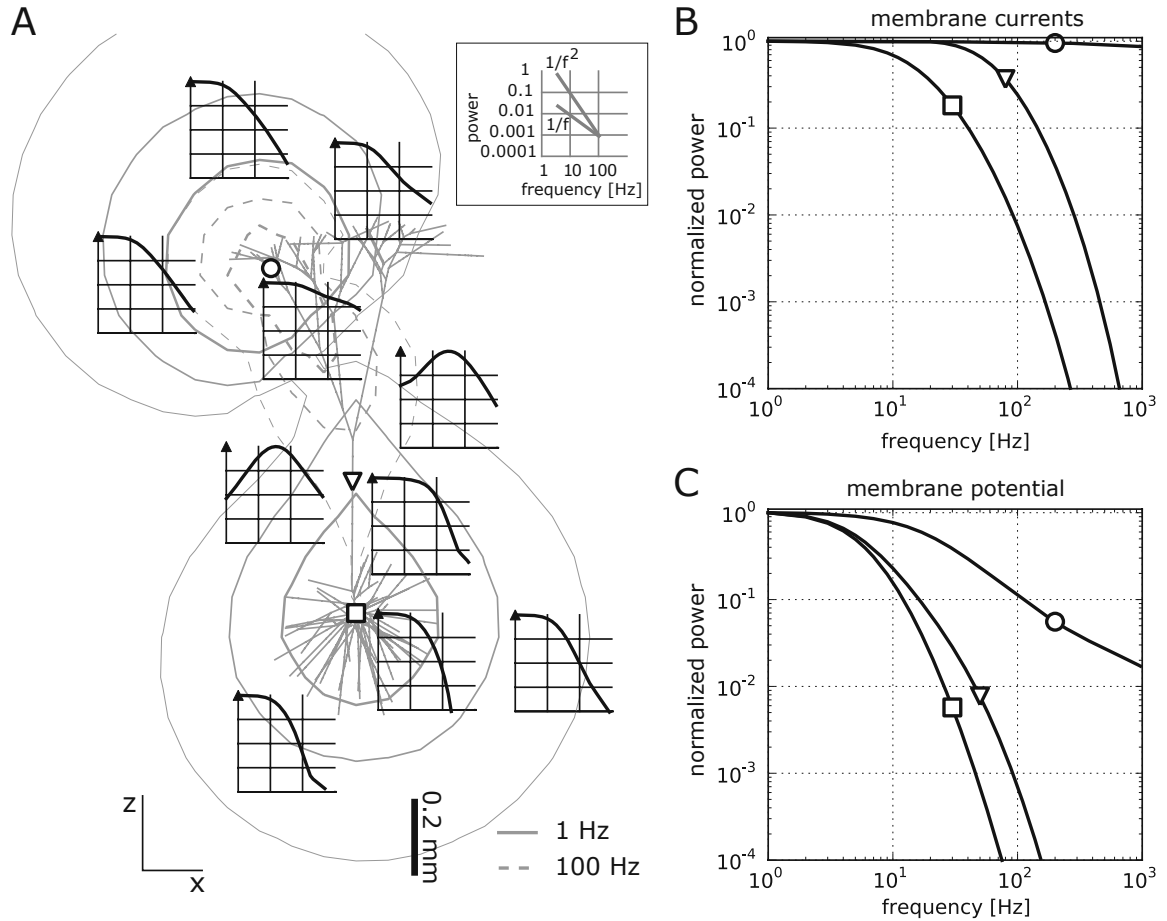

Figure 6: (A) A reconstructed neuron with the morphology of a layer 5 pyramidal cell receives white-noise current at the white circle, at an apical branch. Power spectra at different positions are depicted with scaling shown in the upper right legend. The dashed and solid contour traces display the decay of the 100 Hz power and 1 Hz power, respectively. (B) Double logarithmic power scaling of the membrane currents at locations indicated in the layer 5 pyramidal cell (A), with a square at the soma, triangle at an arbitrary point in the middle, circle at the location of the current injection. (C) illustrates the same as (B) but for the LFP. Reproduced from Lindén et al., 2010

4.4. Modeling frequency filtering

Action potentials are typically regarded to contribute less to the LFP signal, which is often explained by the frequency-filtering properties of the extracellular medium. If the conductive medium acts as a low-pass filter, higher frequencies, produced by action potentials, will be attenuated more steeply than lower frequencies, generated by synaptic events (Bedard et al., 2006a; Pettersen and Einevoll, 2008; Bédard and Destexhe, 2009; Bédard et al., 2004).

Simply computing a two-compartment model does not show a dependency on distance for frequency filtering (Pettersen and Einevoll, 2008). Several causes have been proposed for the frequency-filtering properties of the LFP, but the origin is still being debated. The $1/f^n$ scaling of the LFP power can primarily be explained by the low-pass frequency filtering property of dendritic morphology according to (Lindén et al., 2010; Gold et al., 2006; Pettersen et al., 2008; Pettersen and Einevoll, 2008, Figure 6). Bédard et al. (2010), however, indicated that this only holds for isolated inputs used in the model. When natural

synaptic input trains at many synaptic terminals are modeled the filtering effect disappears. Furthermore, the logarithmic scale is only observed in high frequencies, similar to a model by Bedard et al. (2006b), while there is no frequency scaling at lower frequencies (which is observed in experimental data). Self organized criticality has also been suggested to describe $1/f$ noise (Bedard et al., 2006b). Another explanation suggested that action potentials might generate quadrupoles (Milstein and Koch, 2008) which attenuate more steeply ($1/r^3$) than dipoles ($1/r^2$). Yet another possible source of frequency filtering is the non-homogeneous extracellular space itself (Bédard et al., 2004). The extracellular space is a complex aggregate of fluids (extracellular and intracellular) and membranes (dendrites, axons, myelin, glial cells, etc). While membranes can be viewed as insulators, the fluids are conductive, providing a highly non-homogeneous extracellular conductivity.

Heterogeneous conductivity may also be considered a means to explain the low-pass filtered LFP (Gabriel et al., 1996b; Bédard et al., 2004). Heterogeneous conductivity $\sigma(\omega)$ and permittivity $\epsilon(\omega)$ are assumed to be constant for all frequencies in Eq. 2, rendering it invalid. To solve this, a microscopic approach considering volumes in the order of μm^3 (a volume containing both insulating, membranes, and conducting, fluids, media) can be used in which σ and ϵ are explicitly separated into the Fourier components of the transmembrane currents. A second approach involves a macroscopic model with volumes in the order of mm^3 which averages over the microscopic properties.

4.4.1. Microscopic modeling

Since the extracellular potential is a linear summation of the transmembrane current, a sum over the contributions from all Fourier components will provide the total extracellular potential (Bédard et al., 2004; Brette and Destexhe, 2012; Pettersen and Einevoll, 2008). Using the Maxwell equations Bédard et al. (2004) showed that the extracellular potential in heterogeneous medium follows this equation:

$$\nabla \cdot ((\sigma + i\omega\epsilon)\nabla\phi_\omega) = 0. \tag{6}$$

This equation describes (in Fourier frequency space) the ω-frequency part of the extracellular potential, ϕ_ω, and its dependence on permittivity and conductivity. Because σ and ϵ can be described as a function of their location, the propagation of the LFP through inhomogeneous extracellular space can be calculated. Simulations with this equation show a low-pass filter when σ is high near the membrane and attenuation as the distance from the neuron increases (Bédard et al., 2004).

If we assume a one-compartment current source described in Eq. 1 the extracellular potential at distance R from the source can be written as:

$$\phi_\omega = \frac{I_\omega^f}{4\pi\sigma(R)} \int_R^\infty \frac{1}{r'^2} \cdot \frac{\sigma(R) + i\omega\varepsilon(R)}{\sigma(r') + i\omega\varepsilon(r')} dr' \, , \tag{7}$$

Varying σ and ϵ with location affects the outcome of the integral, displaying different kinds of frequency filtering. If the permittivity and conductivity are constant, the integral reduces to $1/R$ and the equation can be written as Eq. 1 again.

4.4.2. Macroscopic modeling

Another approach uses mean-field models of neuronal activity (Deco et al., 2008; Bédard and Destexhe, 2011). Theoretically, solving Eq. 7 should be sufficient to get the frequency dependence of LFPs. However, the conductivity at a microscopic scale depends on whether a membrane or fluid is considered. Because of the highly non-homogeneous extracellular medium it is impossible to define the electric parameters for each frequency and every point in space yielding the equation unsolvable. The macroscopic formalism proposed by Bédard and Destexhe (2009) incorporates macroscopic measurements naturally, because the Maxwell equations are invariant to change of scale (if σ and ϵ are renormalized) and examines different physical causes for frequency dependence. In order to use a macroscopic model macroscopic electric parameters are defined by averaging the microscopic parameters over a certain volume:

$$\epsilon_\omega^M(\vec{x}) = < \epsilon_\omega(\vec{x}) >_{|Vol} = f(\vec{x}, \omega)$$

and

$$\sigma_\omega^M(\vec{x}) = <\sigma_\omega(\vec{x})>_{|Vol} = g(\vec{x}, \omega) .$$

where the volume Vol at position $\vec{x}$ over which the average is taken equals around 1 mm^3, which is much smaller than the typical cortical volume. Therefore, the macroscopic parameters will be dependent on the position in the brain.

In contrast to the microscopic electric parameters, ϵ_ω^M and σ_ω^M are frequency dependent. In Eq. 6 impedance inequalities can generate a frequency dependence. Intuitively, it seems natural that if a medium has low-pass filtering properties due to inhomogeneities of σ and ϵ, these filtering properties have to remain at a more macroscopic level. This can only be accomplished if the parameters ϵ^M and σ^M are frequency dependent. Thus, even though the electric parameters of a non-homogeneous medium on a microscopic scale are frequency independent, for the macroscopic equations to be consistent average values of the parameters depend on frequency. While a perfectly resistive and homogeneous medium will not produce frequency dependent ϵ^M and σ^M, ionic diffusion, polarization and capacitive effects result in specific frequency-dependencies. A mean-field equation describing the macroscopic extracellular potential over a certain volume $<\phi_\omega>_{|Vol}$ is obtained with this equation:

$$\nabla \cdot ((\sigma_\omega^M + i\omega\epsilon_\omega^M)\nabla < \phi_\omega >_{|Vol}) = 0 . \tag{8}$$

This formula is similar to Eq. 6 for the microscopic situation, but here physical processes (e.g. ionic diffusion, surface polarization, non-homogeneity) can be integrated by using the corresponding frequency dependence of the macroscopic conductivity and permittivity.

It is important to note that the dependency of ϵ_ω^M and σ_ω^M on frequency is described by the Kramers-Kronig relations (Kronig, 1926; Lifshitz et al., 1984; Foster and Schwan, 1995). The permittivity and conductivity should be dependent on each other (governed by these relation) in order to simulate experimental data (Gabriel et al., 1996b; Bedard et al., 2006b; Bédard and Destexhe, 2009).
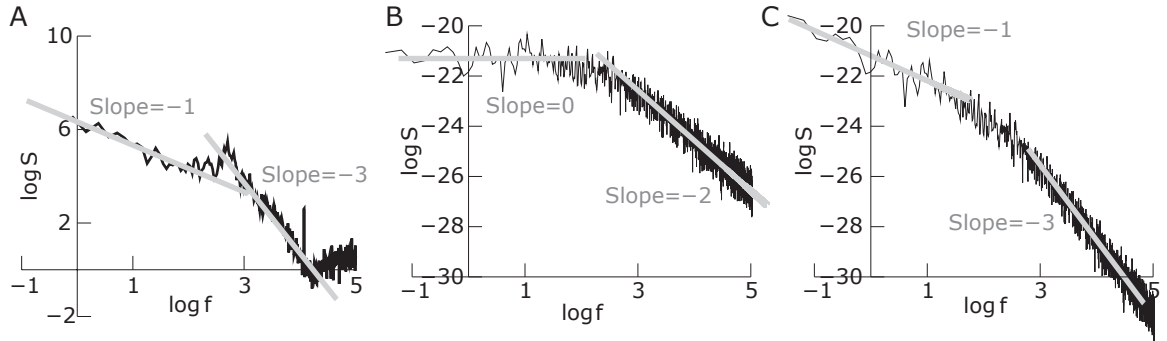

Figure 7: (A) Power spectral density of experimentally recorded LFPs from cat parietal cortex. (B) Attempted reconstruction of the LFP power spectrum calculated from the synaptic current (convolution with unit activity). (C) Accurate simulation of the power spectral density of the experimental data by incorporating ionic diffusion into the model. Reproduced from Bédard and Destexhe, 2009

While ECoG simulations were discussed in Section 4.3, ECoG studies typically do not include more complex models such as the macroscopic model of Eq. 8. Power spectrum density modeling by Miller et al. (2009) showed different power scaling compared with Bedard et al. (2006b). They explained the difference by pointing out that the frequency dependency of passive neuronal tissue (which is key in Bedard et al., 2006b) has been contradicted (Logothetis et al., 2007), who found that the impedance is homogeneous, isotropic (when considering gray matter) and frequency-independent. While the different simulations indeed point towards different scalings, this does not necessarily indicate an absence of tissue filtering (Bédard and Destexhe, 2009). They might rather be explained by the use of different subjects (cat in Bédard and Destexhe vs. human in Miller et al.), modeling formalism and parameters (e.g. electric parameters, postsynaptic kernel parameters).

17

Gabriel et al. (1996b) described the conductivities of various tissues (human and animal, mostly ovine, some porcine) across a relevant frequency range and the extended model incorporates ionic diffusion and electric polarization to account for the different conductivities of cortical tissue (Bédard and Destexhe, 2009). It also reconciles the apparent opposing findings of Gabriel et al. (1996b) and Logothetis et al. (2007). The diffusion-polarization model considers a current flow which can explain the $1/f$ scaling measured in LFP, ECoG and EEG. And, as mentioned earlier, the macroscopic model is invariant under scale changes (if the electromagnetic parameters are adjusted accordingly) and therefore still holds at the larger spatial sampling scale of the ECoG signal.

A way to find out the electric parameters at the scale of ECoG in the model might be iterating the model and optimizing it to find the best power scale fit. To minimize the necessary computing power, certain constraints would need to be introduced, e.g. based on conductivities (Gabriel et al., 1996b), the Kramers-Kronig relations (Kronig, 1926) and the size and distribution of the neural population. The model might have to be expanded to account for macroscale interactions of dipole configurations. Ultimately a more complex forward-model describing the current flow could illuminate the composition and generation of the ECoG signal.

The distribution of charges around a passive cell is influenced by an electric field. The cell is polarized because the positive (extracellular) and negative (intracellular) ions are displaced along the membrane according to the direction of the electric field. Ionic diffusion occurs to establish equilibrium after a neuron receives synaptic input creating extracellular currents as well. Incorporating both mechanisms was shown accurately to simulate the frequency scaling of LFPs recorded in cat parietal cortex (Bédard and Destexhe, 2009). In contrast to Lindén et al. (2010) and Bedard et al. (2006b) the low-frequencies are correctly scaled by this model as well (Figure 7). Taking into account both polarization and ionic diffusion allows one to simulate the conductivities recorded by Gabriel et al. (1996b). The diffusion-polarization model of Bédard and Destexhe (2009) might explain the findings of Logothetis et al. (2007) (no frequency dependence of the extracellular medium) because their methods limit ionic diffusion, which is key in modeling the frequency dependency. For a recent paper on power scaling of microscopic and macroscopic recordings, Pettersen et al. (preprint) comprehensively describe and model power spectral densities (using standard cable theory).

4.5. Contributions of action potentials to the LFP

While spikes are typically assumed to be less prominent in the LFP, they do indeed contribute to the signal. Previously this was shown in studies in which spike trains were extracted from LFP data (which logically indicates a considerable contribution). Furthermore, studies were discussed showing an increase in high-frequency power related to synchronous and frequent spiking activity. However, these studies did not address the signature of action potentials to the extracellular field directly. Belluscio et al. (2012) removed the spiking signature in the visual cortex of a monkey by deconvolving the signal using the spike trains and the mean waveform. Note that this does not remove spikes signatures from neurons farther away (which will not be recognized as single units) or spike induced AHP, which were shown previously to have simi-
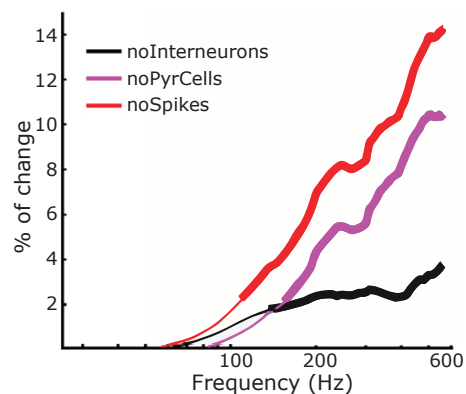

Figure 8: Frequency plotted against % change of power with the bold lines indicating a significant change from the unfiltered LFP. noInterneurons is the curve where interneuron spikes are removed, noPyrCells where pyramidal cell spikes are removed and noSpikes is the curve with all spikes removed. Reproduced from Belluscio et al., 2012

lar temporal scaling to synaptic processes. This way, the AHP component of a spike contributes to the low-frequency spectrum. Nonetheless, the extent of their spike-removal is sufficient to demonstrate a small decrease in high frequencies. With the removal of interneurons a decrease of a few percent in frequency power is observed at high frequencies. Removing all spikes produced a much larger decrease, because the majority of the spikes stem from pyramidal cells (Figure 8).

The high-frequency range, which to a large degree reflects action potentials, has been described previously to decrease with distance. Interestingly, it increases when membranes are tightly packed, i.e. in densely aligned somata or axons (Belluscio et al., 2012). A modeling study in Pettersen and Einevoll (2008)

demonstrated some of these characteristics using a single dendrite with a soma (ball-and-stick neuron) for action potentials (previous examples used synaptic activity or white-noise to drive the field potential). From the ball-and-stick neuron a function is extracted to describe how a membrane potential at the soma can be rewritten as a LFP. They demonstrate different equations (one close to the soma and one for far-fields) explain a low-pass frequency filter dependent on location, with distant locations showing less high-frequency power. Near the soma, high frequencies are enhanced, displaying a sharper extracellular than intracellular spiking signature. Another characteristic demonstrated by the model illustrates how the cross-sectional surface of the dendrites attached to the soma is positively related with the extracellular spiking amplitude. This feature could be used in various recording methods by measuring near neuronal populations with numerous sizable dendrites, thus optimizing the size of the spike signature. The effect of the dendritic arborization can for instance be illustrated by comparing the amplitude of spikes in stellate and pyramidal cells. At a distance of $60\mu m$ the extracellular spiking amplitude of stellate cells is 10 mV while the spike amplitude recorded from a pyramidal cell with an action potential of the same strength and shape was modeled to be 40 mV.

4.6. Population model

Because LFPs do not originate from field signatures of single cells, simulating LFPs generated by a population of neurons is necessary to better understand recorded signals. Pettersen et al. (2008) created a population from 1040 digitally reconstructed morphologies of layer-5 pyramidal neurons arranging them stochastically in a small column, similar to sensory neocortical column. Simulating realistic LFPs required a sparsely distributed synaptic input that was strong enough to create action potentials (40 neurons); and the remaining neurons do receive small input (no spiking). Synaptic input was temporally shifted with a Gaussian function. Apical dendrites predominantly needed to receive excitatory postsynaptic potentials and basal dendrites inhibitory potentials to resemble experimental recordings. EFPs were calculated at 23 positions along a virtual multicontact electrode for 40 trials, each having a randomly computed temporal shift and spatial configuration. The LFP along the column was virtually the same for each trial. The MUA (high-pass filtered at 750-5000 Hz) mainly and quite accurately reflects firing neurons in the proximity of the electrode and shows high variability when comparing across trials. This is expected regarding the random placement and firing of the neurons. Averaging over trials demonstrates the MUA is reproducible (smoothing out some high frequencies due to the stochastic firing patterns) and independent of its synaptic input. The MUA attenuates quickly outside the neuronal population (radial distances $> 200\mu m$), which means the signal is reduced by factor 30 (compared with factor 5 for LFPs). In Section 4.2 results from a comparable population model were used to explain spatial reach of the LFP (Lindén et al., 2011). Three types of populations were modeled build from reconstructed layer-3 pyramidal cells, layer-4 stellate cells and layer-5 pyramidal cells (each population contained of 10,000 neurons).

This approach to modeling populations may be used to simulate well understood brain areas. For example, the projections of input and output of the layers in V1 have been extensively described (Douglas and Martin, 1998, columnar organization of various brain areas reviewed in Mountcastle, 1997). Hagen et al. (2013) describe a $1mm^2$ slice of cat V1 with spike trains generated by leaky integrate-and-fire neuron model and its related LFP calculated with multicompartmental models. The synaptic connectivity and connections within and between layers of the slice (based on Binzegger et al., 2004) is simulated with reconstructed neurons from layer-2 to layer-6.

Ocular dominance columns are an organizational characteristic of V1 with a diameter of $\sim 500\mu m$ in primates (Hubel and Wiesel, 1969) and $730\mu m - 1mm$ in humans (Adams et al., 2007). Another common feature of V1 organization is orientation tuning, which has been widely studied since the work of Hubel and Wiesel (1959). Because orientation columns only span about $\sim 50\mu m$ Berens et al. (2008) were unable to correlate MUA to LFPs in an orientation tuning experiment. At the spatial scale of ocular dominance columns however, MUA and LFPs γ-bands were correlated fairly well. Berens et al.'s conclude that these LFP frequencies reflect activity sampled from an area with a diameter of $500 - 800\mu m$. Note however that, as discussed previously, synchrony is essential for explaining spatial spread, which means the visual stimulation and connectivity in the columns is related to this distance. A study simultaneously measuring epidural ECoG and intracortical activity demonstrated a correlation between ECoG and spikes for a measure of ocular dominance (Toda et al., 2011). Distinguishing between the ocular dominance columns with

epicortical measurements would require high spatial resolution at submillimeter scale, e.g. with micro-ECoG (Viventi et al., 2010; Thongpang et al., 2011). With ECoG electrodes aligned perpendicularly to the dipoles generated by the populations in ocular dominance columns, neighboring columns will contribute relatively little to the signal. At large distances from the dipole, the EFP decays as $1/r^3$ when moving orthogonally from the dipole (compared with $1/r^2$ when moving along a constant angle), indicating the possibility of decoupling the ECoG signals from separate ocular dominance columns to some degree. Creating a population model of two adjacent ocular dominance columns might elucidate which exact scale and input patterns are necessary to optimally differentiate between the columns.

5. Conclusions and future directions

All transmembrane currents give rise to an extracellular voltage which is highly influenced by the morphology of neurons, the cytoarchitecture and the synchrony in the neural networks. A recent surge in interest in the low-frequency spectrum of the extracellular potential, the LFP, is reflected by the increase in analytical methods which show how the LFP provides information that complements the information conveyed by spike trains. Disambiguating the aggregate of contributors to the LFP remains challenging however. One reason concerns the difficulties in constructing an experimental design where different electrophysiological recording techniques or stimuli can be effectively decoupled, since they typically show some degree of interdependency. Furthermore, the traditional approach of distinguishing between frequency bands based on differences of their power is insufficient in several aspects. Global properties of the spectrum (Lisman, 2005), correlations between frequencies (Canolty et al., 2006) or properties independent from power are usually not addressed. A promising way to tackle these issues and efficiently decompose the signal may be by using machine learning and pattern recognition algorithms (Rasch et al., 2008; Liutkus et al., 2011).

A useful approach to differentiate between the neuronal contributions to the LFP, and thus to a better understanding of what information is conveyed by the signal is that using modeling schemes. Numerical modeling can provide quantitative descriptions of the generation of the LFP while incorporating the connectivity, architecture and biophysical mechanisms in a particular region of the brain. Computing the LFP using morphologically accurate reconstructed cells is a rather recent development (Holt and Koch, 1999), but with the increase in computer power, availability of reconstructed neurons (`http://NeuroMorpho.Org`) and the development of software such as NEURON (Carnevale and Hines, 2006), studies using forward-modeling schemes are increasing. Simulating cortical columns or large tissue volumes has been used to describe the propagation of LFPs and spikes. This is essential to develop accurate micro-circuitry that can describe experimental data. Validating models with experimental data with appropriate fitting techniques is essential to obtain the best model (Holmes et al., 2006; Friston et al., 2002). Reconstructing the functional organization of various cortical structures may be used to predict limitations and possibilities of recording methods with different spatial and temporal resolutions. Stimuli could be chosen based on these modeling studies taking into account the synchrony they would evoke, thus creating optimally decoding conditions. For example, to measure very small columns a large evoked potential would cause the signal to spread too wide to distinguish the columns and stimuli eliciting a specific amount of synchrony should be used.

Many non-synaptic processes have been suggested to contribute to the LFP, but most biophysical models currently do not incorporate these mechanisms. While ephaptic effects have been introduced in a modeling study by describing the polarization of passive cells (Bédard and Destexhe, 2009), contributions such as spike afterhyperpolarizations (Buzsáki et al., 1988), glial interactions (Petsche et al., 1984; He et al., 2008) and Ca^{2+} spikes (Helmchen et al., 1999) remain to be incorporated. However, before this is possible a more complete view on biological mechanisms of these processes is necessary.

Due to the complexity and interdependency of the neuronal processes, a promising approach is combining methods with different spatiotemporal accuracy. This multimodal approach involves understanding the measurement physics of the methodologies: characterizing the link between experimental measure and neuronal dynamics to make optimum use of the simultaneously measured recordings. For example, a better understanding of the numerous types of electrodes and the implications of their electric parameters would be needed for effective multimodal recordings (Nelson et al., 2008). The relation between action potentials and synaptic activity is particularly interesting because unit activity at one location will cause synaptic activity at a different site. One measurement of this relationship can be acquired with spike-triggered LFP

averages, which describe the interaction between LFPs and spikes at different recording positions in the neuronal circuitry (Nauhaus et al., 2008; Okun et al., 2010). This line of research is still in a preliminary stage and seems worth exploring further.

Measuring ECoG and spikes simultaneously would allow the use of the simple forward-model used in Miller et al. (convolution of Poisson distributed spikes with a postsynaptic curve kernel). By using this multimodal approach experimental spike trains can be used to feed the model, instead of 6000 presynaptic inputs received by a single simulated neuron. A convolution of the intracortically measured spikes with the postsynaptic kernel might simulate the epicortically recorded ECoG signal. Spiking recorded just below the cortical surface would be expected to simulate the ECoG signal reasonably accurate, but with larger distance this resemblance would decay (Watanabe et al., 2012). Another extension on the methods in (Miller et al., 2009) could be an optimization of the parameters of the shape of the postsynaptic current (rise and decay) to compute the best shape of the kernel. The kernel shape might be dependent on the position of the electrode recording spikes, growing smoother and smaller as the distance increases.

A study measuring LFPs, spikes and ECoG simultaneously in the primary motor cortex of a rat yielded interesting results (Yazdan-Shahmorad et al., 2013). They demonstrated a correlation between high-γ power density of ECoG and unit firing in layers 5 and 6 after electrical stimulation, while the same frequency power of the LFPs correlated with the units in all layers. These types of multimodal findings will assist in working out the connectivity and input distribution necessary for describing experimental data with reconstructed columns in the motor cortex.

Studying the relation between the LFP and network dynamics with neural mass models is yet another important approach to understanding LFP oscillations and spike-LFP interaction (Deco et al., 2008). This kind of population model describes the network activity based on a single dynamical variable. Combining the contributions of these variables in a population with LFP analyses or forward-modeling schemes could elucidate the relative contributions to the recorded potential. Ultimately, future progress requires combining, developing and expanding analyses and modeling schemes to understand the superposition of the multiple neural population signals that give rise to the extracellular potential.

References

Abeles, M., 1991. Corticonics: Neural circuits of the cerebral cortex. Cambridge University Press.

Adams, D. L., Sincich, L. C., Horton, J. C., 2007. Complete pattern of ocular dominance columns in human primary visual cortex. The Journal of Neuroscience 27 (39), 10391–10403.

Adrian, E. D., Moruzzi, G., 1939. Impulses in the pyramidal tract. The Journal of physiology 97 (2), 153.

Adrian, E. D., Zotterman, Y., 1926. The impulses produced by sensory nerve-endings part ii. the response of a single end-organ. The Journal of physiology 61 (2), 151–171.

Anastassiou, C. A., Montgomery, S. M., Barahona, M., Buzsáki, G., Koch, C., 2010. The effect of spatially inhomogeneous extracellular electric fields on neurons. The Journal of neuroscience 30 (5), 1925–1936.

Anastassiou, C. A., Perin, R., Markram, H., Koch, C., 2011. Ephaptic coupling of cortical neurons. Nature neuroscience 14 (2), 217–223.

Arvanitaki, A., 1942. Effects evoked in an axon by the activity of a contiguous one. J. Neurophysiol 5 (2), 89–108.

Barth, D. S., 2003. Submillisecond synchronization of fast electrical oscillations in neocortex. The Journal of neuroscience 23 (6), 2502–2510.

Barth, D. S., Di, S., 1991. Laminar excitability cycles in neocortex. Journal of neurophysiology 65 (4), 891–898.

Bazelot, M., Dinocourt, C., Cohen, I., Miles, R., 2010. Unitary inhibitory field potentials in the ca3 region of rat hippocampus. The Journal of physiology 588 (12), 2077–2090.

Bean, B. P., 2007. The action potential in mammalian central neurons. Nature Reviews Neuroscience 8 (6), 451–465.

Bédard, C., Destexhe, A., 2009. Macroscopic models of local field potentials and the apparent 1/f noise in brain activity. Biophysical journal 96 (7), 2589–2603.

Bédard, C., Destexhe, A., 2011. Generalized theory for current-source-density analysis in brain tissue. Physical Review E 84 (4), 041909.

Bedard, C., Kroeger, H., Destexhe, A., 2006b. Does the 1/f frequency scaling of brain signals reflect self-organized critical states? Physical review letters 97 (11), 118102.

Bédard, C., Kröger, H., Destexhe, A., 2004. Modeling extracellular field potentials and the frequency-filtering properties of extracellular space. Biophysical journal 86 (3), 1829–1842.

Bedard, C., Kröger, H., Destexhe, A., 2006a. Model of low-pass filtering of local field potentials in brain tissue. Physical Review E 73 (5), 051911.

Bédard, C., Rodrigues, S., Roy, N., Contreras, D., Destexhe, A., 2010. Evidence for frequency-dependent extracellular impedance from the transfer function between extracellular and intracellular potentials. Journal of computational neuroscience 29 (3), 389–403.

Belitski, A., Gretton, A., Magri, C., Murayama, Y., Montemurro, M. A., Logothetis, N. K., Panzeri, S., 2008. Low-frequency local field potentials and spikes in primary visual cortex convey independent visual information. The Journal of Neuroscience 28 (22), 5696–5709.

Belluscio, M. A., Mizuseki, K., Schmidt, R., Kempter, R., Buzsáki, G., 2012. Cross-frequency phase–phase coupling between theta and gamma oscillations in the hippocampus. The Journal of neuroscience 32 (2), 423–435.

Berens, P., Keliris, G., Ecker, A., Logothetis, N., Tolias, A., 2008. Comparing the feature selectivity of the gamma-band of the local field potential and the underlying spiking activity in primate visual cortex. Frontiers in systems neuroscience 2.

Binzegger, T., Douglas, R. J., Martin, K. A., 2004. A quantitative map of the circuit of cat primary visual cortex. The Journal of Neuroscience 24 (39), 8441–8453.

Bishop, G., 1936. The interpretation of cortical potentials. In: Cold Spring Harbor Symposia on Quantitative Biology. Vol. 4. Cold Spring Harbor Laboratory Press, pp. 305–319.

Bower, J. M., Beeman, D., 1995. The book of GENESIS: exploring realistic neural models with the GEneral NEural SImulation System. Electronic Library of Science, The.

Bremer, F., 1938. L'activité électrique de l'écorce cérébrale et le problème physiologique du sommeil. Boll Soc Ital Biol Sper 13, 271–290.

Bremer, F., 1944. Aspect theorique de lelectro-encephalographie. Arch. néerl. Physiol. 28, 481–487.

Brette, R., Destexhe, A., 2012. Handbook of neural activity measurement. Cambridge University Press.

Buzsáki, G., Anastassiou, C. A., Koch, C., 2012. The origin of extracellular fields and currentseeg, ecog, lfp and spikes. Nature Reviews Neuroscience 13 (6), 407–420.

Buzsáki, G., Bickford, R. G., Ponomareff, G., Thal, L., Mandel, R., Gage, F. H., 1988. Nucleus basalis and thalamic control of neocortical activity in the freely moving rat. The Journal of neuroscience 8 (11), 4007–4026.

Buzsáki, G., Buhl, D., Harris, K., Csicsvari, J., Czeh, B., Morozov, A., 2003. Hippocampal network patterns of activity in the mouse. Neuroscience 116 (1), 201–211.

Buzsáki, G., Czopf, J., Kondakor, I., Kellenyi, L., 1986. Laminar distribution of hippocampal rhythmic slow activity (rsa) in the behaving rat: current-source density analysis, effects of urethane and atropine. Brain research 365 (1), 125–137.

Buzsaki, G., Penttonen, M., Nadasdy, Z., Bragin, A., 1996. Pattern and inhibition-dependent invasion of pyramidal cell dendrites by fast spikes in the hippocampus in vivo. Proceedings of the National Academy of Sciences 93 (18), 9921–9925.

Cajal, R., 1904. Histologie du systeme nerveux de l'homme et des vertebras. Paris: Maloine 2.

Canolty, R. T., Edwards, E., Dalal, S. S., Soltani, M., Nagarajan, S. S., Kirsch, H. E., Berger, M. S., Barbaro, N. M., Knight, R. T., 2006. High gamma power is phase-locked to theta oscillations in human neocortex. science 313 (5793), 1626–1628.

Carnevale, N. T., Hines, M. L., 2006. The NEURON book. Cambridge University Press.

Caton, R., 1875. Electrical currents of the brain. The Journal of Nervous and Mental Disease 2 (4), 610.

Chan, C., Nicholson, C., 1986. Modulation by applied electric fields of purkinje and stellate cell activity in the isolated turtle cerebellum. The Journal of physiology 371 (1), 89–114.

Chao, Z. C., Nagasaka, Y., Fujii, N., 2010. Long-term asynchronous decoding of arm motion using electrocorticographic signals in monkeys. Frontiers in neuroengineering 3.

Christie, A., Kamen, G., 2010. Short-term training adaptations in maximal motor unit firing rates and afterhyperpolarization duration. Muscle & nerve 41 (5), 651–660.

Contreras, D., Steriade, M., 1995. Cellular basis of eeg slow rhythms: a study of dynamic corticothalamic relationships. The Journal of Neuroscience 15 (1), 604–622.

Cortez, M., Wu, Y., Gibson, K., Snead III, O., 2004. Absence seizures in succinic semialdehyde dehydrogenase deficient mice: a model of juvenile absence epilepsy. Pharmacology Biochemistry and Behavior 79 (3), 547–553.

Creutzfeldt, O. D., Watanabe, S., Lux, H. D., 1966. Relations between eeg phenomena and potentials of single cortical cells. i. evoked responses after thalamic and epicortical stimulation. Electroencephalography and clinical neurophysiology 20 (1), 1–18.

Crone, N. E., Korzeniewska, A., Franaszczuk, P. J., 2011. Cortical gamma responses: searching high and low. International Journal of Psychophysiology 79 (1), 9–15.

Crone, N. E., Miglioretti, D. L., Gordon, B., Lesser, R. P., 1998. Functional mapping of human sensorimotor cortex with electrocorticographic spectral analysis. ii. event-related synchronization in the gamma band. Brain 121 (12), 2301–2315.

Csicsvari, J., Jamieson, B., Wise, K. D., Buzsáki, G., 2003. Mechanisms of gamma oscillations in the hippocampus of the behaving rat. Neuron 37 (2), 311–322.

David, S. V., Malaval, N., Shamma, S. A., 2010. Decoupling action potential bias from cortical local field potentials. Computational intelligence and neuroscience 2010, 7.

Deco, G., Jirsa, V. K., Robinson, P. A., Breakspear, M., Friston, K., 2008. The dynamic brain: from spiking neurons to neural masses and cortical fields. PLoS computational biology 4 (8), e1000092.

Destexhe, A., 1998. Spike-and-wave oscillations based on the properties of gabab receptors. The Journal of neuroscience 18 (21), 9099–9111.

Destexhe, A., Bedard, C., et al., 2012. Do neurons generate monopolar current sources? J. Neurophysiol 108, 953–955.

Di, S., Baumgartner, C., Barth, D. S., 1990. Laminar analysis of extracellular field potentials in rat vibrissa/barrel cortex. Journal of Neurophysiology 63 (4), 832–840.

Douglas, R., Martin, K., 1998. Neocortex.

Douglas, R. J., Martin, K., 1991. A functional microcircuit for cat visual cortex. The Journal of Physiology 440 (1), 735–769.

Du, J., Blanche, T. J., Harrison, R. R., Lester, H. A., Masmanidis, S. C., 2011. Multiplexed, high density electrophysiology with nanofabricated neural probes. PLoS One 6 (10), e26204.

Ebersole, J. S., Pedley, T. A., 2003. Current practice of clinical electroencephalography. Lippincott Williams & Wilkins.

Eccles, J., 1951. Interpretation of action potentials evoked in the cerebral cortex. Electroencephalography and clinical neurophysiology 3 (4), 449–464.

Einevoll, G. T., Kayser, C., Logothetis, N. K., Panzeri, S., 2013. Modelling and analysis of local field potentials for studying the

function of cortical circuits. Nature Reviews Neuroscience 14 (11), 770–785.

Einevoll, G. T., Pettersen, K. H., Devor, A., Ulbert, I., Halgren, E., Dale, A. M., 2007. Laminar population analysis: estimating firing rates and evoked synaptic activity from multielectrode recordings in rat barrel cortex. Journal of neurophysiology 97 (3), 2174–2190.

Foster, K. R., Schwan, H. P., 1995. Dielectric properties of tissues. Handbook of biological effects of electromagnetic fields 2, 25–102.

Friston, K. J., 1994. Functional and effective connectivity in neuroimaging: a synthesis. Human brain mapping 2 (1-2), 56–78.

Friston, K. J., Glaser, D. E., Henson, R. N., Kiebel, S., Phillips, C., Ashburner, J., 2002. Classical and bayesian inference in neuroimaging: applications. Neuroimage 16 (2), 484–512.

Gabriel, S., Lau, R., Gabriel, C., 1996b. The dielectric properties of biological tissues: Ii. measurements in the frequency range 10 hz to 20 ghz. Physics in medicine and biology 41 (11), 2251.

Gail, A., Brinksmeyer, H., Eckhorn, R., 2003. Simultaneous mapping of binocular and monocular receptive fields in awake monkeys for calibrating eye alignment in a dichoptical setup. Journal of neuroscience methods 126 (1), 41–56.

Glickfeld, L. L., Roberts, J. D., Somogyi, P., Scanziani, M., 2009. Interneurons hyperpolarize pyramidal cells along their entire somatodendritic axis. Nature neuroscience 12 (1), 21.

Gold, C., Henze, D. A., Koch, C., Buzsáki, G., 2006. On the origin of the extracellular action potential waveform: a modeling study. Journal of neurophysiology 95 (5), 3113–3128.

Golding, N. L., Jung, H.-y., Mickus, T., Spruston, N., 1999. Dendritic calcium spike initiation and repolarization are controlled by distinct potassium channel subtypes in ca1 pyramidal neurons. The Journal of neuroscience 19 (20), 8789–8798.

Golomb, D., 2007. Neuronal synchrony measures. Scholarpedia 2 (1), 1347, revision #123400.

Gratiy, S. L., Pettersen, K. H., Einevoll, G. T., Dale, A. M., 2013. Pitfalls in the interpretation of multielectrode data: on the infeasibility of the neuronal current-source monopoles. Journal of neurophysiology 109 (6), 1681–1682.

Hagen, E., Stavrinou, M. L., Linden, H., Tetzlaff, T., van Albada, S., Dahmen, D., Diesmann, M., Gruen, S., Einevoll, G. T., 2013. Hybrid scheme for modeling lfps from spiking cortical network models. BMC Neuroscience 14 (Suppl 1), P119.

Halnes, G., Østby, I., Pettersen, K. H., Omholt, S. W., Einevoll, G. T., 2013. Electrodiffusive model for astrocytic and neuronal ion concentration dynamics. PLoS computational biology 9 (12), e1003386.

Hansel, D., Sompolinsky, H., 1996. Chaos and synchrony in a model of a hypercolumn in visual cortex. Journal of computational neuroscience 3 (1), 7–34.

He, B. J., Snyder, A. Z., Zempel, J. M., Smyth, M. D., Raichle, M. E., 2008. Electrophysiological correlates of the brain's intrinsic large-scale functional architecture. Proceedings of the National Academy of Sciences 105 (41), 16039–16044.

Heldman, D. A., Wang, W., Chan, S. S., Moran, D. W., 2006. Local field potential spectral tuning in motor cortex during reaching. Neural Systems and Rehabilitation Engineering, IEEE Transactions on 14 (2), 180–183.

Helmchen, F., Svoboda, K., Denk, W., Tank, D. W., 1999. In vivo dendritic calcium dynamics in deep-layer cortical pyramidal neurons. Nature neuroscience 2 (11), 989–996.

Herculano-Houzel, S., Collins, C. E., Wong, P., Kaas, J. H., 2007. Cellular scaling rules for primate brains. Proceedings of the National Academy of Sciences 104 (9), 3562–3567.

Hodgkin, A. L., Huxley, A., Katz, B., 1952. Measurement of current-voltage relations in the membrane of the giant axon of loligo. The Journal of physiology 116 (4), 424.

Holmes, W. R., Ambros-Ingerson, J., Grover, L. M., 2006. Fitting experimental data to models that use morphological data from public databases. Journal of computational neuroscience 20 (3), 349–365.

Holt, G. R., Koch, C., 1999. Electrical interactions via the extracellular potential near cell bodies. Journal of computational neuroscience 6 (2), 169–184.

Hubel, D., Wiesel, T., 1969. Anatomical demonstration of columns in the monkey striate cortex. Nature 221 (5182), 747–750.

Hubel, D. H., Wiesel, T. N., 1959. Receptive fields of single neurones in the cat's striate cortex. The Journal of physiology 148 (3), 574.

Hubel, D. H., Wiesel, T. N., 1962. Receptive fields, binocular interaction and functional architecture in the cat's visual cortex. The Journal of physiology 160 (1), 106.

Jasper, H., Kershman, J., 1941. Electroencephalographic classification of the epilepsies. Archives of Neurology & Psychiatry 45 (6), 903–943.

Jefferys, J., 1995. Nonsynaptic modulation of neuronal activity in the brain: electric currents and extracellular ions. Physiological reviews 75 (4), 689–723.

Kahana, M. J., Seelig, D., Madsen, J. R., 2001. Theta returns. Current opinion in neurobiology 11 (6), 739–744.

Kajikawa, Y., Schroeder, C., 2011. How local is the local field potential? Neuron 72 (5), 847–858.

Kang, J., Jiang, L., Goldman, S. A., Nedergaard, M., 1998. Astrocyte-mediated potentiation of inhibitory synaptic transmission. Nature neuroscience 1 (8), 683–692.

Katzner, S., Nauhaus, I., Benucci, A., Bonin, V., Ringach, D., Carandini, M., 2009. Local origin of field potentials in visual cortex. Neuron 61 (1), 35–41.

Koch, C., Segev, I., 2000. The role of single neurons in information processing. nature neuroscience 3, 1171–1177.

Kopell, N., Ermentrout, B., 2004. Chemical and electrical synapses perform complementary roles in the synchronization of interneuronal networks. Proceedings of the national academy of sciences of the United States of America 101 (43), 15482–15487.

Kornhuber, H., Becker, W., Täumer, R., Hoehne, O., Iwase, K., 1969. Cerebral potentials accompanying voluntary movements in man: readiness potential and reafferent potentials. Electroencephalography and clinical neurophysiology 26 (4), 439.

Kreiman, G., Hung, C., Kraskov, A., Quiroga, R., Poggio, T., DiCarlo, J., 2006. Object selectivity of local field potentials and spikes in the macaque inferior temporal cortex. Neuron 49 (3), 433–445.

Kreuz, T., Mormann, F., Andrzejak, R. G., Kraskov, A., Lehnertz, K., Grassberger, P., 2007. Measuring synchronization in coupled model systems: A comparison of different approaches. Physica D: Nonlinear Phenomena 225 (1), 29–42.

Kronig, R., 1926. On the theory of dispersion of x-rays. Journal of Optical Society Of America 1626 (12), 547–556.

Kruse, W., Eckhorn, R., 1996. Inhibition of sustained gamma oscillations (35-80 hz) by fast transient responses in cat visual cortex.

Proceedings of the National Academy of Sciences 93 (12), 6112.

Larkum, M. E., Nevian, T., Sandler, M., Polsky, A., Schiller, J., 2009. Synaptic integration in tuft dendrites of layer 5 pyramidal neurons: a new unifying principle. Science 325 (5941), 756–760.

Leski, S., Lindén, H., Tetzlaff, T., Pettersen, K. H., Einevoll, G. T., 2013. Frequency dependence of signal power and spatial reach of the local field potential. PLoS computational biology 9 (7), e1003137.

Leski, S., Pettersen, K. H., Tunstall, B., Einevoll, G. T., Gigg, J., Wójcik, D. K., 2011. Inverse current source density method in two dimensions: inferring neural activation from multielectrode recordings. Neuroinformatics 9 (4), 401–425.

Leski, S., Wójcik, D. K., Tereszczuk, J., Świejkowski, D. A., Kublik, E., Wróbel, A., 2007. Inverse current-source density method in 3d: reconstruction fidelity, boundary effects, and influence of distant sources. Neuroinformatics 5 (4), 207–222.

Leuthardt, E. C., Schalk, G., Wolpaw, J. R., Ojemann, J. G., Moran, D. W., 2004. A brain–computer interface using electrocortico-graphic signals in humans. Journal of neural engineering 1 (2), 63.

Liebe, S., Hoerzer, G. M., Logothetis, N. K., Rainer, G., 2012. Theta coupling between v4 and prefrontal cortex predicts visual short-term memory performance. Nature neuroscience 15 (3), 456–462.

Lifshitz, E., Pitaevskii, L., Landau, L., 1984. Electrodynamics of continuous media: Volume 8.

Lindén, H., Pettersen, K. H., Einevoll, G. T., 2010. Intrinsic dendritic filtering gives low-pass power spectra of local field potentials. Journal of computational neuroscience 29 (3), 423–444.

Lindén, H., Tetzlaff, T., Potjans, T. C., Pettersen, K. H., Grün, S., Diesmann, M., Einevoll, G. T., 2011. Modeling the spatial reach of the lfp. Neuron 72 (5), 859–872.

Lisman, J., 2005. The theta/gamma discrete phase code occuring during the hippocampal phase precession may be a more general brain coding scheme. Hippocampus 15 (7), 913–922.

Liu, J., Newsome, W., 2006. Local field potential in cortical area mt: stimulus tuning and behavioral correlations. The Journal of neuroscience 26 (30), 7779–7790.

Liutkus, A., Badeau, R., Richard, G., 2011. Gaussian processes for underdetermined source separation. Signal Processing, IEEE Transactions on 59 (7), 3155–3167.

Logothetis, N., Kayser, C., Oeltermann, A., 2007. In vivo measurement of cortical impedance spectrum in monkeys: implications for signal propagation. Neuron 55 (5), 809–823.

Logothetis, N., Pauls, J., Augath, M., Trinath, T., Oeltermann, A., et al., 2001. Neurophysiological investigation of the basis of the fmri signal. Nature 412 (6843), 150–157.

Logothetis, N. K., 2002. The neural basis of the blood–oxygen–level–dependent functional magnetic resonance imaging signal. Philosophical Transactions of the Royal Society of London. Series B: Biological Sciences 357 (1424), 1003–1037.

Logothetis, N. K., Wandell, B. A., 2004. Interpreting the bold signal. Annu. Rev. Physiol. 66, 735–769.

Lorente, d. N., 1947. A study of nerve physiology. Studies from the Rockefeller institute for medical research. Reprints. Rockefeller Institute for Medical Research 131, 1.

Magri, C., Mazzoni, A., Logothetis, N. K., Panzeri, S., 2012. Optimal band separation of extracellular field potentials. Journal of neuroscience methods 210 (1), 66–78.

Manning, J. R., Jacobs, J., Fried, I., Kahana, M. J., 2009. Broadband shifts in local field potential power spectra are correlated with single-neuron spiking in humans. The Journal of neuroscience 29 (43), 13613–13620.

Mehring, C., Nawrot, M. P., de Oliveira, S. C., Vaadia, E., Schulze-Bonhage, A., Aertsen, A., Ball, T., 2004. Comparing information about arm movement direction in single channels of local and epicortical field potentials from monkey and human motor cortex. Journal of Physiology-Paris 98 (4), 498–506.

Miller, K. J., 2010. Broadband spectral change: evidence for a macroscale correlate of population firing rate? The Journal of Neuroscience 30 (19), 6477–6479.

Miller, K. J., Sorensen, L. B., Ojemann, J. G., den Nijs, M., 2009. Power-law scaling in the brain surface electric potential. PLoS computational biology 5 (12), e1000609.

Milstein, J., Mormann, F., Fried, I., Koch, C., 2009. Neuronal shot noise and brownian $1/f^2$ behavior in the local field potential. PLoS One 4 (2), e4338.

Milstein, J. N., Koch, C., 2008. Dynamic moment analysis of the extracellular electric field of a biologically realistic spiking neuron. Neural computation 20 (8), 2070–2084.

Mitzdorf, U., 1985. Current source-density method and application in cat cerebral cortex: investigation of evoked potentials and eeg phenomena. Physiological reviews 65 (1), 37–100.

Moruzzi, G., Magoun, H., 1949. Brain stem reticular formation and activation of the {EEG}. Electroencephalography and Clinical Neurophysiology 1 (14), 455 – 473.
URL http://www.sciencedirect.com/science/article/pii/0013469449902199

Mountcastle, V. B., 1997. The columnar organization of the neocortex. Brain 120 (4), 701–722.

Nauhaus, I., Busse, L., Carandini, M., Ringach, D., 2008. Stimulus contrast modulates functional connectivity in visual cortex. Nature neuroscience 12 (1), 70–76.

Nelson, M. J., Pouget, P., Nilsen, E. A., Patten, C. D., Schall, J. D., 2008. Review of signal distortion through metal microelectrode recording circuits and filters. Journal of neuroscience methods 169 (1), 141–157.

Nicholson, C., Freeman, J., 1975. Theory of current source-density analysis and determination of conductivity tensor for anuran cerebellum. Journal of neurophysiology 38 (2), 356–368.

Niedermeyer, E., da Silva, F. L., 2005. Electroencephalography: basic principles, clinical applications, and related fields. Lippincott Williams & Wilkins.

Nielsen, K. J., Logothetis, N. K., Rainer, G., 2006. Dissociation between local field potentials and spiking activity in macaque inferior temporal cortex reveals diagnosticity-based encoding of complex objects. The Journal of neuroscience 26 (38), 9639–9645.

Nunez, P. L., 2006. Electric fields of the brain: the neurophysics of EEG. Oxford University Press.

Okun, M., Naim, A., Lampl, I., 2010. The subthreshold relation between cortical local field potential and neuronal firing unveiled by intracellular recordings in awake rats. The Journal of Neuroscience 30 (12), 4440–4448.

Perez Velazquez, J. L., Carlen, P. L., 2000. Gap junctions, synchrony and seizures. Trends in neurosciences 23 (2), 68–74.

Pesaran, B., Pezaris, J. S., Sahani, M., Mitra, P. P., Andersen, R. A., 2002. Temporal structure in neuronal activity during working memory in macaque parietal cortex. Nature neuroscience 5 (8), 805–811.

Petsche, H., Pockberger, H., Rappelsberger, P., 1984. On the search for the sources of the electroencephalogram. Neuroscience 11 (1), 1–27.

Pettersen, K. H., Devor, A., Ulbert, I., Dale, A. M., Einevoll, G. T., 2006. Current-source density estimation based on inversion of electrostatic forward solution: effects of finite extent of neuronal activity and conductivity discontinuities. Journal of neuroscience methods 154 (1), 116–133.

Pettersen, K. H., Einevoll, G. T., 2008. Amplitude variability and extracellular low-pass filtering of neuronal spikes. Biophysical journal 94 (3), 784–802.

Pettersen, K. H., Hagen, E., Einevoll, G. T., 2008. Estimation of population firing rates and current source densities from laminar electrode recordings. Journal of computational neuroscience 24 (3), 291–313.

Pettersen, K. H., Lindén, H., Tetzlaff, T., Einevoll, G. T., 2013. On $1/f^\alpha$ power laws originating from linear neuronal cable theory: power spectral densities of the soma potential, transmembrane current and single-neuron contribution to the eeg. arXiv preprint arXiv:1305.2332.

Peyrache, A., Dehghani, N., Eskandar, E. N., Madsen, J. R., Anderson, W. S., Donoghue, J. A., Hochberg, L. R., Halgren, E., Cash, S. S., Destexhe, A., 2012. Spatiotemporal dynamics of neocortical excitation and inhibition during human sleep. Proceedings of the National Academy of Sciences 109 (5), 1731–1736.

Pravdich-Neminsky, V., 1913. Ein versuch der registrierung der elektrischen gehirnerscheinungen. Zbl Physiol 27, 951–960.

Pritchard, W. S., 1992. The brain in fractal time: 1/f-like power spectrum scaling of the human electroencephalogram. International Journal of Neuroscience 66 (1-2), 119–129.

Purcell, E. M., Morin, D. J., 2013. Electricity and magnetism. Cambridge University Press.

Purves, D., Augustine, G. J., Fitzpatrick, D., Hall, W. C., Lamantia, A.-S., McNamara, J. O., Williams, S. M., 2004. Neuroscience.

Radman, T., Su, Y., An, J. H., Parra, L. C., Bikson, M., 2007. Spike timing amplifies the effect of electric fields on neurons: implications for endogenous field effects. The Journal of Neuroscience 27 (11), 3030–3036.

Rall, W., 1962. Electrophysiology of a dendritic neuron model. Biophysical journal 2 (2), 145–167.

Rall, W., Shepherd, G. M., 1968. Theoretical reconstruction of field potentials and dendrodendritic synaptic interactions in olfactory bulb. J. Neurophysiol 31 (6), 884–915.

Ramsey, N., Aarnoutse, E., Vansteensel, M., 2014. Brain implants for substituting lost motor function: State of the art and potential impact on the lives of motor-impaired seniors. Gerontology 60 (4), 366–372.

Rasch, M. J., Gretton, A., Murayama, Y., Maass, W., Logothetis, N. K., 2008. Inferring spike trains from local field potentials. Journal of neurophysiology 99 (3), 1461–1476.

Ray, S., Crone, N. E., Niebur, E., Franaszczuk, P. J., Hsiao, S. S., 2008a. Neural correlates of high-gamma oscillations (60–200 hz) in macaque local field potentials and their potential implications in electrocorticography. The Journal of Neuroscience 28 (45), 11526–11536.

Ray, S., Hsiao, S. S., Crone, N. E., Franaszczuk, P. J., Niebur, E., 2008b. Effect of stimulus intensity on the spike–local field potential relationship in the secondary somatosensory cortex. The Journal of Neuroscience 28 (29), 7334–7343.

Ray, S., Maunsell, J. H., 2010. Differences in gamma frequencies across visual cortex restrict their possible use in computation. Neuron 67 (5), 885–896.

Ray, S., Maunsell, J. H., 2011. Different origins of gamma rhythm and high-gamma activity in macaque visual cortex. PLoS biology 9 (4), e1000610.

Riera, J. J., Ogawa, T., Goto, T., Sumiyoshi, A., Nonaka, H., Evans, A., Miyakawa, H., Kawashima, R., 2012. Pitfalls in the dipolar model for the neocortical eeg sources. Journal of neurophysiology 108 (4), 956–975.

Sanes, J. N., Donoghue, J. P., 1993. Oscillations in local field potentials of the primate motor cortex during voluntary movement. Proceedings of the National Academy of Sciences 90 (10), 4470–4474.

Schiller, J., Major, G., Koester, H. J., Schiller, Y., 2000. Nmda spikes in basal dendrites of cortical pyramidal neurons. Nature 404 (6775), 285–289.

Schwartz, A. B., Cui, X. T., Weber, D. J., Moran, D. W., 2006. Brain-controlled interfaces: movement restoration with neural prosthetics. Neuron 52 (1), 205–220.

Siegel, M., König, P., 2003. A functional gamma-band defined by stimulus-dependent synchronization in area 18 of awake behaving cats. The Journal of neuroscience 23 (10), 4251–4260.

Steriade, M., 2003. Neuronal substrates of sleep and epilepsy. Cambridge University Press.

Steriade, M., Contreras, D., 1998. Spike-wave complexes and fast components of cortically generated seizures. i. role of neocortex and thalamus. Journal of neurophysiology 80 (3), 1439–1455.

Stumpf, M. P., Porter, M. A., 2012. Critical truths about power laws. Science 335 (6069), 665–666.

Takeuchi, S., Ziegler, D., Yoshida, Y., Mabuchi, K., Suzuki, T., 2005. Parylene flexible neural probes integrated with microfluidic channels. Lab on a Chip 5 (5), 519–523.

Tarantola, A., 2005. Inverse problem theory and methods for model parameter estimation. siam.

Thongpang, S., Richner, T. J., Brodnick, S. K., Schendel, A., Kim, J., Wilson, J. A., Hippensteel, J., Krugner-Higby, L., Moran, D., Ahmed, A. S., et al., 2011. A micro-electrocorticography platform and deployment strategies for chronic bci applications. Clinical EEG and Neuroscience 42 (4), 259–265.

Toda, H., Suzuki, T., Sawahata, H., Majima, K., Kamitani, Y., Hasegawa, I., 2011. Simultaneous recording of ecog and intracortical neuronal activity using a flexible multichannel electrode-mesh in visual cortex. Neuroimage 54 (1), 203–212.

Viventi, J., Kim, D.-H., Moss, J. D., Kim, Y.-S., Blanco, J. A., Annetta, N., Hicks, A., Xiao, J., Huang, Y., Callans, D. J., et al., 2010. A conformal, bio-interfaced class of silicon electronics for mapping cardiac electrophysiology. Science translational medicine 2 (24), 24ra22–24ra22.

Wang, C., Ulbert, I., Schomer, D., Marinkovic, K., Halgren, E., 2005. Responses of human anterior cingulate cortex microdomains

to error detection, conflict monitoring, stimulus-response mapping, familiarity, and orienting. The Journal of neuroscience 25 (3), 604–613.

Watanabe, H., Sato, M.-a., Suzuki, T., Nambu, A., Nishimura, Y., Kawato, M., Isa, T., 2012. Reconstruction of movement-related intracortical activity from micro-electrocorticogram array signals in monkey primary motor cortex. Journal of neural engineering 9 (3), 036006.

Wong, R., Prince, D., Basbaum, A., 1979. Intradendritic recordings from hippocampal neurons. Proceedings of the National Academy of Sciences 76 (2), 986–990.

Woodin, M. A., Ganguly, K., Poo, M.-m., 2003. Coincident pre-and postsynaptic activity modifies gabaergic synapses by postsynaptic changes in cl¡ sup¿-¡/sup¿ transporter activity. Neuron 39 (5), 807–820.

Xing, D., Yeh, C., Shapley, R., 2009. Spatial spread of the local field potential and its laminar variation in visual cortex. The Journal of Neuroscience 29 (37), 11540–11549.

Yazdan-Shahmorad, A., Kipke, D. R., Lehmkuhle, M. J., 2013. High gamma power in ecog reflects cortical electrical stimulation effects on unit activity in layers v/vi. Journal of neural engineering 10 (6), 066002.

Zhang, Y., van Drongelen, W., Kohrman, M., He, B., 2008. Three-dimensional brain current source reconstruction from intra-cranial ecog recordings. NeuroImage 42 (2), 683–695.